1-28-2015

IDENTIFICATION OF ELECTROREFINER AND CATHODE PROCESSING FAILURE MODES AND DETERMINATION OF SIGNATURE-SIGNIFICANCE FOR INTEGRATION INTO A SIGNATURE BASED SAFEGUARDS FRAMEWORK FOR PYROPROCESSING

Philip Lafreniere

Philip Lafreniere

Candidate

Nuclear Engineering

Department

This thesis is approved, and it is acceptable in quality and form for publication:

Approved by the Thesis Committee:

Edward Blandford, Chairperson

Edward Arthur

Benjamin Cipiti

Anil Prinja

IDENTIFICATION OF ELECTROREFINER AND CATHODE PROCESSING FAILURE MODES AND DETERMINATION OF SIGNATURE-SIGNIFICANCE FOR INTEGRATION INTO A SIGNATURE BASED SAFEGUARDS FRAMEWORK FOR PYROPROCESSING

by

PHILIP LAFRENIERE

B.S. NUCLEAR ENGINEERING, UNIVERSITY OF NEW MEXICO, 2013

THESIS

Submitted in Partial Fulfillment of the

Requirements for the Degree of

Master of Science

Nuclear Engineering

The University of New Mexico

Albuquerque, New Mexico

December, 2014

ACKNOWLEDGEMENTS

I would like to acknowledge several individuals without whom this research would have not been possible. First and foremost my advisor Edward Blandford, who introduced me to the subject of pyroprocessing safeguards and provided me guidance throughout my thesis project.

I would also like to acknowledge my committee members. I would like to first thank Edward Arthur of the University of New Mexico for his perspective and assistance that he provided. I would also like to acknowledge Benjamin Cipiti of Sandia National Lab, without whose initial work, analyses, and advice, this work may not have been carried out. Finally, I would like to thank Anil Prinja for agreeing to serve on my committee and providing a useful perspective on the neutronics modeling performed in this thesis.

In addition, this work would not have been possible without the assistance of several other collaborators. I cannot express enough gratitude to Robert Hoover of INL who taught me most of the basic knowledge that I posses about electrochemistry while doing his postdoctoral work at UNM. I would also like to thank Michael Simpson and Devin Rappleye from the University of Utah for their support and collaboration on this work. Their involvement has been instrumental to its direction and ultimate completion. Finally, I would like to acknowledge Il Soon Hwang of Seoul National University and Man-Sung Yim of KAIST for developing the REFIN/ERAD codes and allowing our research team to use them.

Finally, I would like to say thank you to my family, friends, and God who kept me motivated and focused throughout this entire process. In particular, I would like to acknowledge Bobby Sena who grammatically reviewed my thesis for submission.

IDENTIFICATION OF ELECTROREFINER AND CATHODE PROCESSING FAILURE MODES AND DETERMINATION OF SIGNATURE-SIGNIFICANCE FOR INTEGRATION INTO A SIGNATURE BASED SAFEGUARDS FRAMEWORK FOR PYROPROCESSING

By

Philip Lafreniere

B.S., Nuclear Engineering, University of New Mexico, 2013

M.S., Nuclear Engineering, University of New Mexico, 2014

ABSTRACT

The traditional method of safeguarding nuclear facilities, nuclear material accountancy (NMA), faces many challenges when applied to pyroprocessing facilities. To aid in the safeguarding of these facilities, process monitoring (PM) is being investigated as a complementary method to NMA. PM takes general process data, such as density, current etc., and applies it to safeguards through the use of a statistical framework. Signature Based Safeguards (SBS), a proposed statistical framework for the application of PM techniques, identifies anomalous scenarios and subsequently identifies and detects their respective PM signatures from a system of sensors. This work focuses both on assisting SBS through identifying anomalous scenarios, and on the computer modeling of these failure modes and the PM signatures for them. The anomalous scenarios investigated were mechanical failure modes with potential safeguards-significance as they could lead to the deposition of plutonium and other actinides in the

final uranium product ingot. The signatures of these anomalous scenarios were primarily radiation signatures from a coincidence counter that is used to analyze the final ingots. Several different failure modes were identified for both the electrorefiner and the cathode processor. The signatures for these failure modes were then determined by coupling two separate computer models. The first model is a FORTRAN-based electrorefiner code named ERAD capable of modeling the mass transport of metals within an electrorefiner. The second model was an MCNP-based simulation of the Canberra JCC-31 High Level Neutron Coincidence Counter. First, the identified failure modes were simulated by changing ERAD inputs. ERAD calculated an elemental mass composition at the cathode which was then used as the final ingot composition. The final ingot composition was analyzed for single and double neutron coincidence count rates using the MCNP model. The results demonstrate significant radiation signatures for the presence of plutonium as a result of the electrorefiner failure modes. Signatures from cathode processor failure modes were weak and thus warrant future investigation of better detectors for integration into a SBS framework.

TABLE OF CONTENTS

LIST OF FIGURES

LIST OF TABLES

1. INTRODUCTION

Electrochemical reprocessing, or pyroprocessing, is a proposed method for the recycling of used nuclear fuel (UNF) [1]. Pyroprocessing utilizes electrochemistry to separate uranium from UNF and consolidate it into a fuel form for utilization in a fast metal reactor. Pyroprocessing is designed to treat fuels from both light water reactors (LWR) and fast metal reactors. However, it is challenging to apply traditional nuclear safeguard methods such as the mass tracking method, nuclear material accountancy (NMA). New methods utilizing process monitoring (PM) are being developed to increase confidence in NMA measurements [2]. One of these new proposed methodologies is known as signature based safeguards (SBS) [3].

SBS aggregates signals from a pyroprocessing facility to determine whether or not diversion of nuclear materials has occurred. Thus, determination of signals associated with diversion scenarios and off normal operational that may lead to improper mass tracking. Hence, false alarms must be investigated.

This thesis details extensive work into signature determinations and the conclusions. This chapter provides an introduction to traditional NMA safeguards and PM-based safeguards. In addition, pyroprocessing and its specific unit operations are also discussed. Challenges in safeguarding pyroprocessing are detailed. Finally, Motivations for this work are given, and the concluding paragraph outlines the organization of this thesis.

1.1 SAFEGUARDS OVERVIEW

1.1.1 Safeguards Definitions

Safeguards are integral to the design and operation of any commercial nuclear facility. According to the International Atomic Energy Agency (IAEA), which is responsible for implementation and continuing inspection of safeguards, the definition of safeguards is, "The timely detection of a diversion of significant quantity (SQ) of nuclear material from peaceful nuclear activities" [4]. SQ refers only to nuclear materials classified as special nuclear material (SNM) consisting of different materials with fissile or fertile qualities. A table with the values of SQ for various SNM is depicted in Table 1 below.

Table 1- List of Significant Quantities and their Associated Special Nuclear Material **[4]**

SNM	SQ
Pu	8 kg
U-233	8 kg
HEU (U-235 > 20%)	25 kg U-235
LEU (U-235 < 20%)	75 kg U-235
Natural U	10 Mt
Depleted U	20 Mt
The	20 Mt

Safeguard measurements are typically taken in the framework of a measurement method known as NMA which utilizes a mass balance to determine the difference of material coming into a facility versus the amount being removed. This mass balance is illustrated by Equation 1 [2] below:

$$MB = I_{in} + T_{in} - T_{out} - I_{out}, \quad (1)$$

where MB is material balance, I_{in} is the inventory at the beginning of the process, I_{out} is the inventory at the end of the process, T_{in} is inventory being transferred into the process, and T_{out} is the inventory being transferred out of the process. Thus, proper accountancy must occur at all points throughout a process. The goal is to ensure that the value of MB is equal to 0 with a detection probability (DP) of loss equal to 0.95[2]. This goal is met when the total uncertainty is less than the quotient of 1 SQ divided by 3.3.

The inability to meet these uncertainty requirements may lead to one of two different kinds of errors. The first type of error is known as a type I error, which occurs when measurements indicate that diversion has occurred when in fact it has not. This happens in two different manners. The first is a false alarm, which is the first alarm raised to indicate diversion at the safeguarded facility when it has not actually occurred [4]. The second is a false positive, which is when the IAEA inspectors cannot verify whether or not diversion occurred. These errors are particularly important as they hold up plant throughput and are most sensitive to safeguards measurements with high uncertainties.

The second type of safeguard error associated with safeguarding a nuclear facility is known as a type II error. This occurs when an alarm has failed to raise despite the fact that diversion has occurred [4]. These errors have great safeguards implications, but have

less impact on the overall throughput of a plant because the plant does not have an alarm from which it is shutdown and investigated.

1.1.2 Challenges with NMA

Challenges with applying NMA arise from attaining the high level of statistical confidence with the measurements being performed [2]. NMA is most effective when applied to commercial facilities that transport and account for material in bulk forms. This is because when materials are in bulk form they can be monitored and measured as discrete units. As they are discrete units, seals and gross inventory counts of total number of units can be used to monitor if material has been diverted. These discrete units of bulk material include but are not limited to items such as new and UNF assemblies as well as tanks of enriched UF_6 gas [5]. These gross inventory measurements have been aided by improved containment and surveillance techniques (C/S) and improved detection technologies to determine if unauthorized alterations have been made to the bulk material. These technologies include advanced seals and passive radiation detectors. With these technologies, NMA can be applied with high accuracy within these facilities. NMA, however, can face several challenges when applied to reprocessing facilities [1].

NMA faces difficulties when it is applied to reprocessing facilities, as the confidence levels attained in the mass balances applied to these facilities do not meet the required confidence set forth by the IAEA. This is because throughput is very high and involves separation of plutonium from uranium in most cases that must be accounted for. As the SQ of plutonium is low, the mass balance uncertainty must be low. For example, if the uncertainty was to be as low as 0.3% and throughput of plutonium is large such as

1000 kg during a balance period, the greatest diversion it could register with the required confidence is 11.5 kg, which is still greater than 1 SQ and does not fulfill the IAEA safeguards goals [2]. For this reason, measurement technologies that currently exist, which cannot match the hypothetical 0.3%, cannot estimate masses of plutonium and uranium in irradiated and reprocessed fuels to the necessary confidences and thus NMA alone is not a valid method for safeguarding SNM.

These challenges with NMA when applied to reprocessing are evident in the case of the Japanese reprocessing plant at Rokkasho [6]. The Rokkasho plant was one of the first major aqueous reprocessing plants to be developed for commercial purposes that required safeguards due to Japan being a member of the NPT. Due to the multiple process streams and insensitive measurements, safeguarding the plant became a challenge and one that delayed and complicated the construction of Rokkasho [6]. To demonstrate their facility as being safeguardable, Rokkasho operators and engineers continually added measurement and sampling technologies to the plant throughout its construction. These new safeguards measures produced new complications for the operators monitoring the facility to attain a material balance at any time needed [6]. Due to these safeguards challenges and several engineering challenges, the Rokkasho plant has yet to become operational.

1.1.3 PM and NRTA Overview

To address these challenges with applying NMA to reprocessing technologies, two different approaches have been proposed [2][7]. These two approaches are known as process monitoring (PM) and near real time accountancy (NRTA). Both of these

approaches could be useful in increasing safeguards confidence for applications to reprocessing technologies.

NRTA is an extension of the mass balance method common to NMA. It differs from NMA, however, as the periods over which the mass balances occur are shorter. For example, most statistical investigations, however, compare the differences between annual and monthly mass balances [7]. Despite seemingly beneficial in concept, studies by Avenhaus and Jausch demonstrated that for optimal operator protracted diversion of nuclear material, the detection probability (DP) was greater for the annual balance periods as opposed to the monthly ones [8]. However, further statistical studies on NRTA utilizing Page's joint sequential tests have demonstrated that NRTA can provide high DP for abrupt diversion of SNM. The Page's joint test studies also demonstrated DP's of protracted diversion that are higher than those attained by annual NMA balance measurements but still may not be sufficient to attain the confidence required by the IAEA [7]. Current modeling efforts have been made to model pyroprocessing for NRTA and use joint Page's test for analysis [1][7]. These analyses have demonstrated that NRTA, if optimized with daily material balances, can provide the necessary confidence in safeguards measurements. However, NRTA requires unattainably low (with current mass measurement technologies) mass quantification uncertainties to attain the measurement confidence required by the IAEA [1]. Thus, NRTA is not immediately applicable to reprocessing facilities, but could be applied in the future. PM is a set of additional methods for assisting safeguards. PM involves using process measurements to determine if off normal operations indicative of material diversion are occurring. These measurements also aid the facility in ensuring it is operating as intended from an

operations perspective. Typical PM measurements include basic quantities such as temperature, masses and volume of materials, and radiation measurements [3]. These measurements themselves do not inform safeguards but when placed within a statistical architecture can be applicable. There are two major proposed methods for applying PM data. The first is a pattern recognition-based approach [2][7] and the other is a system-centric approach [2][3]. The system-centric approach is also known as SBS. The work of this thesis assists in the further development and understanding of SBS.

PM can be applied to safeguards in one of three ways [2]. The first is where NMA is utilized as the primary safeguards measure, with PM being used as a secondary measure for performing tasks such as assisting in resolving alarms. The second is where PM is the primary measure for taking material inventory and tracking. The final is where PM and NDA operate with equal application to tracking inventory and the results of both are utilized in reaching a conclusion. The methods for SBS discussed in this thesis were investigated to perform in this final kind of assistance.

The pattern recognition approach involves taking data over time from process monitoring techniques and applying sequential tests such as Page's test to determine if large diversions or changes in material quantity have occurred given a certain diversion from the mean value between data points [2]. The Page statistic test has an alarm threshold that above which a large diversion of material is indicated. This method has shown that when combined with NMA, the DP of diversion of material is significantly increased.

SBS utilize a system of sensors and a data integration and interpretation (DII) algorithms to determine if anomalous scenarios are occurring [3][9]. This is performed through the collection of data throughout the process using sensors located at each unit operation. These sensors vary in terms of type and use and some examples of these sensors are seen in Table 2 [3]. These sensors are arranged within the SBS framework to indicate exactly what is occurring at a given part of the plant at both an indicated time as well as over a specified period of time. Each of these sensors registers data as being either normal or off-normal. This data is labeled as *signatures* of either normal or off-normal operation. In the case of measurements such as density or temperature, the data can be registered by the sensor as being off-normal in the forms of low or high. SBS involves identifying what sequence of off-normal signals indicate anomalous operations and thus register an alarm if they occur and the DII modules register the data as being indicative of this sequence.

Table 2- Examples of PM Measurements as Applied to Electrochemical Reprocessing

Sensor Technology	Description
Gas mass flow meter	Volume of Oxygen gas released into off gas system in oxide reduction
Electrical Power Supply	Coulombs of Electric Charge Passed in Electrorefiner (Coulombs)
NDA	Dose of Product from Electrorefiner
Electronic Balance	Mass of Electrowinning product metal (kg)
Double Bubbler	Density of Molten Salt (g/cm^3)

The framework of SBS involves several different modeled levels when it is computationally simulated. The lowest layer is the modeling of each of the unit operations in the process [9]. This layer models the transport of material in each unit operation and can simulate discrete off normal operations [9]. The next level is the sensors monitoring the operations. These sensors register the data and give it to the next level of the framework, the DII analysis module for the given operation [9]. This module then integrates the data for that given time period or event for that given operation to the uppermost level of the framework, which is the system wide DII integrating the data for each event from each of the operational modules. This uppermost DII module then makes the decision to raise an alarm if an anomalous scenario has appeared to have occurred from the integration of the event data or register the event as having occurred within the parameters of normal operation [9].

Computational simulations for the SBS framework have historically been applied to both pyroprocessing and aqueous reprocessing facility models. Anomalous scenarios and the signal sequences are determined [3, 9] and then the simulation is run for a facility for a given number of operational cycles over a prescribed time. During the simulation, there are a fixed number of anomalous scenarios that occur. Each sensor has a pre-determined probability of proper classification, misclassification, and misdetection. The system of sensors is tuned to the prescribed anomalous scenarios and the simulation run. For the case of perfect sensor health and prescribed anomalous scenarios, the DP of these anomalous scenarios is very high [9]. However, the DP changes depending on the value of these probabilities for the sensors. As the sensors became more uncertain, the total DP reduced and the DII was assigned a metric known as the average normalized error

(ANE). The ANE is a measurement of the error of the DII to detect diversion. For various anomalous scenarios, the ANE differs depending on the sensors involved. The ANE when measured in some anomalous scenarios fell outside of the 95% confidence interval [9]. In addition, the number of anomalies detected tends to be an overestimation leading to an increased number of false alarms [9]. Both of these results are undesirable, but could be improved through improved sensor technologies. With improved sensor technology, these errors could be reduced and fall into the range that would be needed to be properly applied as a complementary method to NMA.

Additional runs were made in which the probabilities and uncertainties of the sensors were not changed, but some were assumed to fail [3]. In this case, an increased false alarm probability was registered. This increased number of false alarms increased with the number of sensors assumed to fail. Sensor health, uncertainty, and their ability to identify signatures are of the upmost importance to the proper implementation of SBS.

1.1.4 Safeguard Implications of Process Failures

Though often thought as more of an operational concern, process failures throughout a reprocessing facility also have potential resounding safeguards implications. Failure modes in process equipment can lead to improper or insufficient transport of materials within a process, which causes issues for mass tracking. Failure modes highlight the problems of NMA with respect to reprocessing as it will most likely not be able to assess the transit of mass with high enough accuracy and thus generate a false alarm. This false alarm can develop further into a false positive error which is of even greater significance.

Thus, understanding what failure modes can occur and their implications for generating safeguards errors is important.

1.2 PYROPROCESSING OVERVIEW

1.2.1 Pyroprocessing History

Electrochemical separation of nuclear material is a process that has been known and investigated for quite some time. The production of UO_2 from molten UO_2Cl_2 using electrochemistry was first discovered at the end of the 19^{th} century [10]. After this discovery, research into the development of electrochemical production of fuel was performed primarily in the United States. Brookhaven National Lab (BNL), Los Alamos National Labs (LANL), and Oak Ridge National Labs (ORNL) all lead early research in separations of uranium from salt for fuel from their metal fuel reactors [10]. This salt separations work gave rise to the current extraction process seen today. The first major efforts to extract heavy metal from spent fuel in electrorefiner equipment occurred at LANL in the early 1960s. This process utilized NaCl-KCl eutectic and was utilized to extract 1.6 tons of high purity plutonium metal [10].

The most prominent work in early pyroprocessing is the work carried out by Argonne National Lab (ANL) at their Idaho site [11]. The first efforts at ANL involved the fuel of the EBR-II reactor whose fuel was processed via pyroprocessing in the mid to late 1960s [11]. The other effort that led to the current understanding of pyroprocessing was that to treat the fuel from the Integral Fast Reactor (IFR). This was the first instance where a LiCl-KCl salt eutectic was used for the processing, the most common salt eutectic in current designs [10]. The current electrorefining model involving a fuel basket

with a metal cathode that dendrites of uranium are transported to arose from this work [10, 11].

Electrochemical reprocessing continues to progress in the United States at Idaho. Pyroprocessing is used to treat metal blanket fuel resulting from EBR-II that is significantly depleted uranium or natural uranium [11]. The Mark IV and Mark V electrorefiner were designed for this purpose.

Internationally, electrochemical reprocessing is of the most interest to the Republic of Korea (ROK). The Korea Atomic Energy Research Institute (KAERI) is currently investigating pyroprocessing as the favored method with dealing with the back end of the nuclear fuel cycle [12]. Much research has involved the design of the unit operations of the pyroprocessing, and KAERI even generated its own engineering scale demonstration facility [12]. This demonstration facility is known as the PyRoprocess Inactive integrated DEmonstration (PRIDE) Facility and treats no actual UNF.

Japan and the European Union (EU) have also expressed significant interest in the application of electrochemical reprocessing to the nuclear fuel cycle [10, 13]. In Japan, the Central Research Institute of Electric Power Industry (CRIEPI) has been at the forefront of pyroprocessing research. CRIEPI has developed its own electrorefining capabilities to process actinides and has seen reasonable success [13]. CRIEPI looks to continually develop pyroprocessing for the purpose of commercial use [13]. There exists efforts throughout the EU to develop pyroprocessing capabilities; however, one project of particular interest partners nine different countries with the purpose of developing chemical separations of UNF. This project is known as the Actinide Recycling by

Separation and Transmutation (ACSEPT) [14]. Like the other organizations already discussed, the ASCEPT project has developed its own technological designs for pyrochemical separations including its own electrorefiner design [14].

This history demonstrates that pyroprocessing is a popular subject of investigation for the processing of UNF. For this reason, the development of safeguards should be closely integrated with technological development and facility design as to prevent issues similar to those at Rokkasho.

1.2.2 Pyroprocessing Description

Though there are many facility designs proposed for pyroprocessing, the basic sequence of unit operations within them does not typically differ between them [15]. A flow sheet of this sequence of operations for used oxide fuel is seen in Figure 1.

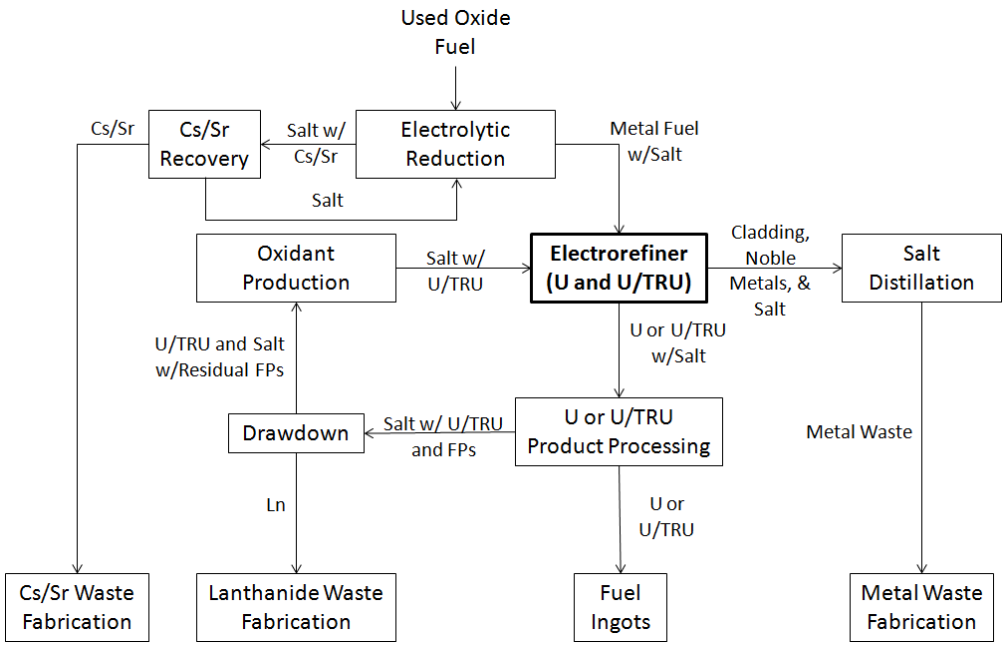

Figure 1- Pyroprocessing Flow sheet for Oxide Fuels

For a plant processing oxide fuel, the input is used fuel assemblies from commercial light water reactors (LWR). These assemblies are chopped into smaller pieces free of cladding and placed within a basket. This basket is lowered into an electroreducer that contains a LiCl-KCl salt bath. Here, through electrochemical reactions where the basket acts as the cathode and the salt acts as the anode, gaseous products specifically oxygen as well as Cs/Sr is removed and transported out of the fuel. The Cs/Sr is consolidated into its own waste form that can be tracked for the purpose of NMA verification.

After removal from the electroreducer, the basket is then lowered into another salt bath within an electrorefiner. Here, through electrochemical reactions where the basket acts as the anode and there is a cathode present, uranium is transported from the basket acting as an anode and deposited at a cathode in the form of dendrites. The active products dissolve into the salt and the cladding and noble metals remain within the basket itself. Both the cathode and the anodic product are left with salt entrained, and both products are transported to processing equipment to have the salt distilled off. The remains after salt distillation of the anode generate a metal waste form that is then assessed, and the uranium metal forms its own consolidated fuel ingot that can be used in later fabrication of fuel for use in a liquid metal reactor (LMR). The salt distilled off as well as some remaining in the electrorefiner is then placed in a drawdown stage during which lanthanides are removed and oxidant production occurs within the salt before being returned to the ER. In addition, U/TRU products ingots form their own consolidated ingot; however, the method by which the U/TRU product is recovered is

still under debate as to whether or not to use a liquid cadmium cathode (LCC). By inspecting the waste forms and consolidated ingots from each of these steps, one can make conclusions about the mass throughput of a facility.

1.2.3 Safeguard Challenges associated with Pyroprocessing

There are multiple unique challenges associated with safeguarding pyroprocessing. The first challenge is that, unlike an aqueous reprocessing facility, there is no input accountability tank to take accurate measurements of the spent fuel inventory after it has been delivered to the facility upfront [1]. This is due to the fact that dissolution and separation of the fuel occur in the same step, i.e. in the electrorefiner, as opposed to aqueous plants where the UNF is dissolved in one specialized dissolver tank and the separations occurs in a separate chemical process tank that the dissolved fuel is pumped into. In order to keep a proper mass balance, the input inventory must be a very accurate measurement or else NMA will most likely not be able to measure with the acceptable accuracy the total mass balance of the plant. To combat these issues with NMA, three measurement schemes have been devised for the inventory. The first two involve quantifying measurements of both UNF assemblies as well as measurements of shredded fuel. Though these measurements are useful, the uncertainties of these measurements are typically high and would likely be unacceptable in the framework of NMA [1]. The other method proposed are measurements done to spent fuel power after a process of voloxidation has occurred up front on the UNF assemblies [1]. This voloxidation process would serve both as a method for removing volatile products and tritium, but also as a type of input accountability tank except with powdered fuel instead

of dissolved fuel. Research has demonstrated that this will most likely not be better in terms of uncertainty, but new methodologies for measurement of the powder may reduce the uncertainty.

The other major issue with safeguarding pyroprocessing that arises is in its inability to have a plant flushout [1]. Plant flushouts occur when the entire plant is shutdown and all material removed and measured thus effectively closing the material balance and effectively determining whether or not diversion has occurred. In a pyroprocessing plant, performing a flushout for the purpose of NMA is not feasible. This is due to the sheer size of the pyroprocessing plants as well as the need to keep salt and actinides in the electrorefiner so that the transport of actinides continues as their presence in the salt is necessary for transport [1]. Removing products would reduce the throughput and make a pyroprocessing facility significantly less efficient.

To address these issues, these new methodologies for aiding NMA such as NRTA and PM have to be applied. How they may be applied and how effective they can be requires further investigation. The motivation of this work comes from the need to determine the applicability of PM to addressing pyroprocessing safeguards specifically because of these challenges.

1.3 Motivation and Approach

1.3.1 Motivation for SBS Signature Identification

As discussed previously, SBS has demonstrated itself as a strong candidate for implementing of PM methods into commercial facilities. To implement SBS into an

actual commercial setting, identifying and modeling signatures is of the upmost importance. This work looked to identify signatures with the ultimate goal of reducing Type I safeguards errors. As discussed previously, operational failure modes can easily lead to situations in mass transfer that could result in false alarms and, with it, false positives. This work looked to reduce the false positive rate by identifying multiple scenarios under which this type of false alarm could occur. This was achieved through a process known as Failure Modes and Effects Analysis (FMEA) first developed by the National Aeronautics and Space Administration (NASA) used for analyzing failure modes and their effects [16]. FMEA performs its work in four steps. The first is to identify the system boundary, which in the case of this work was the electrorefiner, cathode processor, and final ingot casting stages and the associated sensors with it. The second is to identify the boundary and describe each component in the boundary. The third is to identify the potential failure modes. The fourth is to determine the probability, severity, and risk of each potential failure mode [17]. This thesis covers the first three steps and investigated the risk implications of the fourth step.

By being able to identify the failure modes, the signatures from the sensors associated with these failure modes could be investigated. By knowing these signatures, the ability to resolve false alarms would be increased as the DII would be better able to indicate the reason the alarm and thus aid NMA in this resolution. This would in theory significantly reduce the false positives encountered and thus allow the pyroprocessing facility to operate with greater fluency and less safeguards risk.

Another motivation for signature identification also deals with the current limitations and assumptions of the computational model. The current modeling efforts

make assumptions about sensor uncertainty and health [3, 9]. By investigating signatures and sensor modeling the actual ability for these sensors to misclassify or misdetect can be quantified value thus lending to more accurate results from a system centric model. This in turn could lead to the further demonstration of SBS as being an adequate PM-based approach to aiding NMA in safeguarding pyroprocessing facilities. The work of this thesis involves a computational effort to determine safeguards-significant signatures and sensor characteristics for addressing these problems.

1.3.2 General Overview of Approach

As actual experiments and operations could not be performed on a commercial scale, this work was performed through computer modeling. This was done by a loose coupling of two separate computer codes. As this work focused on failure modes in the ER and the subsequent cathode processor, a model and the assumptions for both was developed. To simulate ER throughput, a computer code called Enhanced REFIN with Anodic Dissolution (ERAD) was utilized to simulate mass transport in the ER during a variety of operating conditions. These operating conditions changed depending on a given failure mode analyzed. The cathodic product as result of the mass transport calculation could then be analyzed by a subsequent simulation of a non-destructive assay (NDA) detector to determine what radiation signatures may exist and with what measurement uncertainty. There are many different advanced NDA instruments available in the safeguards arena, ranging from passive gamma detectors to active neutron counting methods. For this work, the modeled detector was the JCC-31 HLNCC, a LANL-

developed, Canberra distributed detector for coincidence counting [18]. This detector was modeled in MCNPx using tallies that allowed for the computation of expected singles and doubles counts from the detector. These simulated counts provide the radiation signatures of interest to be integrated into an SBS framework. This detector was selected as it was heavily documented in the public literature as well as it bore great resemblance to current NDA counting devices under investigation by KAERI for safeguarding SNM [18, 19]. The weak coupling of these two codes provides key insights into these important signatures for integration into an SBS framework.

1.4 Organization of Thesis

This document provides a comprehensive overview of the work undertaken in the signature determination for failure modes determined for both electrorefining and for cathode processing. It is organized in the following manner. Chapter 2 provides an extensive discussion of the technology of both the ER and the CP and discusses the multiple different failure modes that were identified to be possible for both of these technologies. Chapter 3 focuses on the computer models used and developed for both the ER operation and radiation detection measurements of the final consolidated ingot. Chapter 4 gives an overview of the methodology undertaken for the purpose of coupling the two separate computer models. Chapter 5 provides the results of the signature determination work for the ER failure modes. Chapter 6 provides the results of the signature determination work for the determined CP failure modes. Finally, Chapter 7 provides a summary of the work, motivation, results, and final conclusions drawn.

2. PYROPROCESSING EQUIPMENT FAILURE MODES

As discussed previously, pyroprocessing requires multiple steps that utilize advanced process equipment. It is important from a systems perspective to note that none of the complex process equipment designed for pyroprocessing is immune from operational failure. For this reason, understanding the potential manners in which equipment can fail and the overall impact of these failures is crucial for the successful operation for an advanced system such as that of a pyroprocessing plant. Work has been undertaken for this thesis to identify these potential failure modes and analyze their consequences from a safeguards perspective. As process failures can potentially lead to the production of signals that would indicate an alarm in a SBS framework, understanding how to properly identify what failure may have occurred can help in resolving the alarm and reducing the probability of Type I safeguard errors. Thus failure modes with potential safeguards implications were analyzed in this work for electrorefining and cathode processing[20]. This chapter discusses the equipment involved in detail as well as the potential failure modes that were identified.

2.1 ELECTROREFINER FAILURE MODES

2.1.1 Electrorefiner Background

The electrorefiner is a critical stage of electrochemical reprocessing. During this stage, uranium is separated from the chopped fuel for the purpose of producing a final product ingot. Many designs have been developed for electrorefiners over the past 50 years. These many designs differ in key design aspects, but all operate under the same

concepts and theory. Figure 2 depicts one of the most referenced designs along with the labeling of many common parts of an ER, the Mark IV electrorefiner developed by Argonne National Laboratory [11, 21].

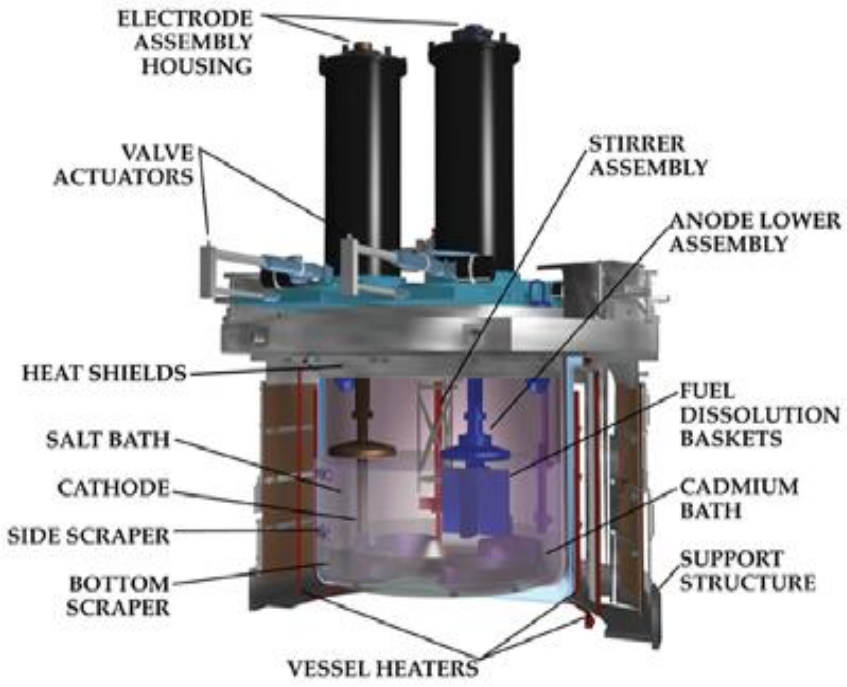

Figure 2- Diagram of Mark-IV Electrorefiner [22]

Most designs of the pyroprocessing ER involve similar conventions and operations. A bath of a eutectic salt, in all common designs LiCl-KCl, is heated by some form of heating element exterior to the bath [12, 14, 21, 23]. In some designs, there is cadmium pool below this salt bath. A fuel dissolution basket (FDB) with the dissolved fuel to be processed is submerged into a salt bath as the first step of operating an electrorefiner [12, 14, 21, 23]. This basket acts as an anode and is rotated by an agitator housed in an assembly above the salt bath. A salt stirrer also rotates to generate

movement of the salt [12, 14, 21, 23]. An electric current is passed through the electrolyte within the electrorefiner that results in the transport of actinides into the salt with noble metals remaining in the anode basket. With proper operation, the uranium product is transported to the cathode where it is deposited on its surface. The other actinides should remain in the salt; however, actinides in the anode basket near the interior of the mass of shredded fuel may not electrolytically separate into the salt. In addition, depending on the operating conditions and potential within the electrorefiner the other active products can transport to the cathode. The cathode also rotates to generate a diffusion layer for mass transport. The cathode differs in the material it is manufactured with between designs. The ANL developed designs utilize a stainless steel cathode for their Mark-IV electrorefiner and concentric stainless steel tubes for their Mark-V design [11, 21]. The electrorefiner developed by KAERI utilizes multiple graphite rods [12, 24]. These graphite rods are chosen as the dendritic cathode deposits fall off on their own into a basket that collects them by vibrations of the cathode. CRIEPI's ER utilizes a solid stainless steel cathode tube [23]. These various cathodes rotate. This rotation occurs to generate the diffusion layer for mass transfer to. The deposited product is then removed from the surface of the cathode for processing. Again this differs depending on design. ANL's designs remove the cathode and then scrape the product off outside the ER equipment [21]. CRIEPI's scrapes using an in-situ scraper into a fuel basket at the bottom of the ER [23]. KAERI's design as stated before, if operating normally, allows for the dendrites to fall off the cathode naturally.

2.1.2 ER Failure Modes

By using this design information, failure modes that are both general for every designed ER and failure modes specific to a given ER could be identified. The failure modes determined were poorly characterized anodic feedstock, temperature variations within the ER, change in rotational speed of electrodes and/or salt stirrer, decreased electrode submersion depth, electrical shorting of the electrodes, and catching of integrated cathode scraper. Further details are described in the following paragraphs.

Poorly characterized anodic feedstock is the result of a misunderstanding of the composition of the UNF within the anodic basket. The composition of the salt and what species dissolve into it are heavily affected by the input composition. Accurate mass measurements are challenging and there are high uncertainties associated with these measurements (typically greater than 5% in magnitude [1]). Most initial fuel estimations are a result of computer burnup programs; however, these programs posses bias that makes them difficult to apply to an actual commercial facility. If the composition of the anode and salt is difficult to characterize and differs significantly from what is expected, the species dissolved into the salt and deposited at the cathode are affected. In addition, the necessary operating conditions of the ER are affected. A higher actinide concentration in the salt can lead to co deposition of TRU at the cathode depending on the operating conditions. For this reason, measurements of both the salt and chopped fuel are continuously being evaluated to gain better accuracy of UNF compositions [1].

The initial composition of the feedstock can also be altered due to incomplete oxide reduction in the electroreducer for the case of chopped ceramic fuels. The presence

of oxygen will make it challenging for the eutectic to oxidize the fuel thus causing more actinides to remain in the anodic basket and be transferred to the metal waste form. This transference to the location where it is not supposed to be makes safeguards through NMA challenging.

Temperature variations in the ER could be the result of several different failure modes. The first is the failure of one or multiple heating elements in the ER vessel wall. Another is a loss of onsite power that causes the heating elements in the ER to cease to operate. A final manner in which this could occur is due to asymmetric heating where one heating element is providing a greater temperature of heating compared to a different heating element in a different portion of the ER vessel. Temperature variations are significant failure modes as it alters the fundamental parameters required by the chemistry of electrorefining such as the diffusivity and solubility of ionic species. In addition, it affects the thermodynamic and kinetic aspects of the reactions within the ER at the electrodes. If these fundamental chemical processes change, the compositions of all three portions of the ER (anode, salt, and cathode) will be different than what was predicted thus adding to challenges in mass tracking.

Change in rotational speed of the electrode would be the result of a failure of the motor rotating the electrode, a failure of the agitator device causing the rotation, or a loss of power for the supply of the motor itself for any of the electrodes. A change in electrode speed is important to understand as it would affect the diffusion layer thickness for transport. This in turn would alter the current, rate of oxidation and/or reduction of the species in the electrorefiner. This change could lead to active species besides uranium to deposit at the cathode, which would provide challenges with mass tracking of materials in

pyroprocessing. If the salt stirrer rotation changes for similar reasons as the electrodes, the homogeneity of the salt in the ER is compromised and this could result in uneven deposition at the cathode.

A decreased electrode submersion depth occurs as a result of either a sticking or jamming of the electrode equipment or a lower than normal salt bath level in the ER due to removal and insufficient replacement of salt from the ER during the drawdown and oxide productions stages. A decreased electrode submersion depth results in a lower surface area, which affects the effective surface area of the electrode. This affects mass transfer, the total current density, and the reactions rate of the species in the ER.

The electrical shorting of the electrodes is due to the reduced uranium product forming as dendrites on the cathode. This has the potential to produce electrical shorting paths. This is a failure mode that has been observed at the Mark IV reactor at INL for the portion between the anode basket and the ER vessel equipment [25]. This electrical shorting will lead to deposition of U/TRU at locations in the ER other than the cathode such as the vessel wall. This provides challenges when trying to safeguard material via mass tracking. In addition, the efficiency of the ER is affected and thus it becomes an operations issue as well. Thus, proper monitoring of an ER during operations and proper scraping of the cathode is a must.

The failure mode of the catching and subsequent jamming of an integrated cathode scraper only applies to ERs that feature an in-situ scraper such as the one present in the CRIEPI design [23]. The mechanism that scrapes the dendrites off the cathode has the potential to catch on the growing deposits thus stopping the deposit of dendrites into

the in-situ dendrite basket and affecting operational parameters. This will affect the surface area, which changes the rates of reaction at the electrodes as well as the current density, which results in similar safeguard challenges to the other failure modes where co-deposition occurs as mass movement is not as expected.

2.2 CATHODE PROCESSOR FAILURE MODES

2.2.1 Cathode Processing Background

Cathode processing is the step immediately following the electrorefiner. In this step the dendritic product from the ER cathode is processed so that the salt left entrained in it from the ER is removed. The remaining product is then consolidated into a metal ingot for future fuel fabrication. This is done by a two step process. The first step involves the uranium dendrites being placed within a process crucible with the salt entrained. This product is then distilled in a high temperature, air evacuated environment so that the salt from the ER is removed and the dendritic products remains. This distillation can occur due to the difference in vapor pressures between the salt and the metal product. After this the second step occurs, the dendritic product is then heated to a high temperature and melted into a consolidated ingot.

This two step process has been generated two major designs of note. The first process created by ANL combines both steps into the same process equipment [26]. A diagram of this piece of equipment is seen in Figure 3. The other design is that designed at KAERI [27]. This separates the two steps into two separate pieces of equipment. Distillation occurs in a distillation column, while the ingot consolidation has its own

melting and pouring equipment for the ingot fabrication. A computer rendered image of the design of the ingot consolidation equipment is in Figure 4.

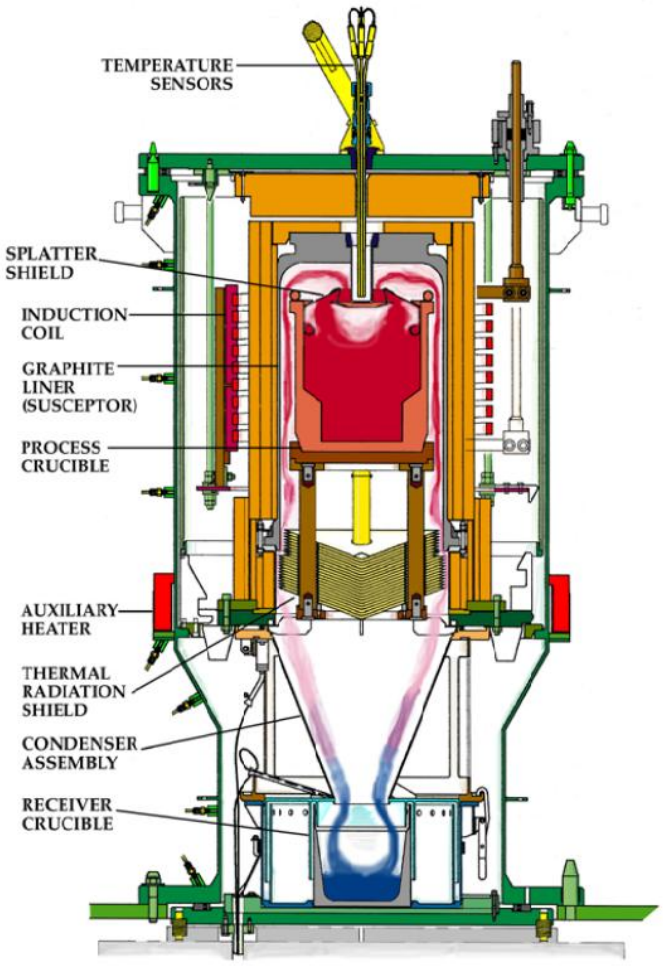

Figure 3- Diagram of ANL's Cathode Processing Equipment Design [26]

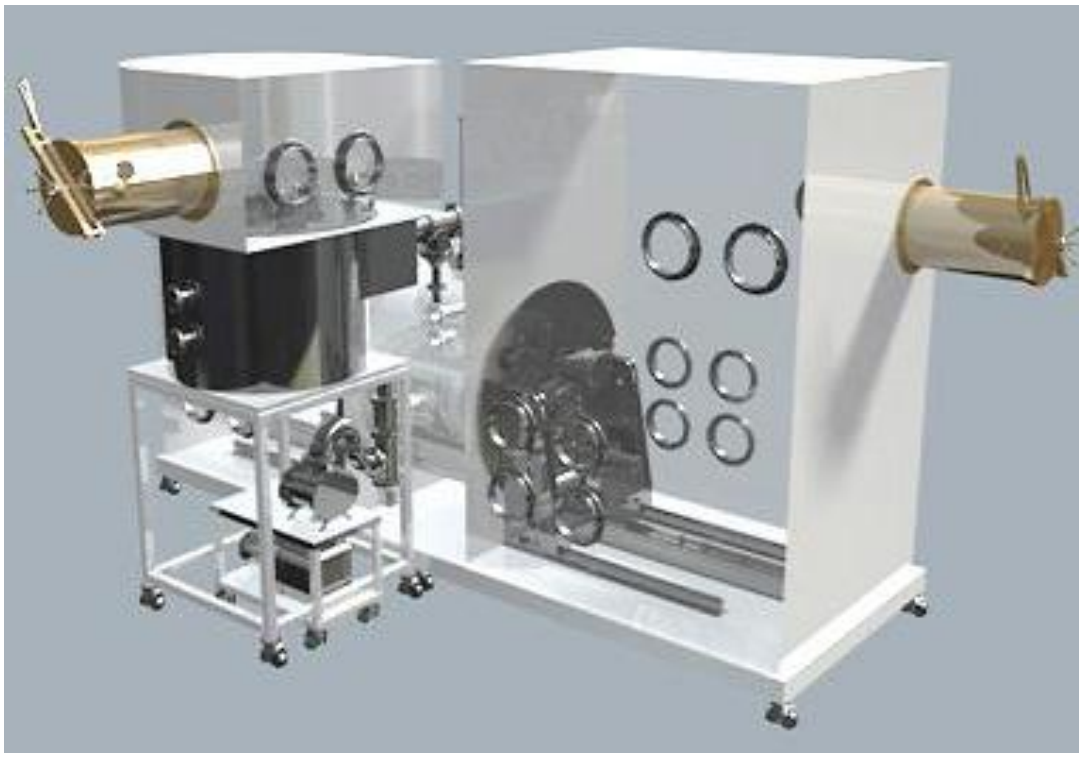

Figure 4- Diagram of KAERI's Ingot Consolidation Equipment [27]

2.2.2 CP Failure Modes

Several different failure modes have been identified both for the distillation step and the consolidation and ingot casting step. These failure modes are for the most part the same for either design. These failure modes include poorly characterized feedstock for both steps in the process, temperature variation failure modes that applies to both steps in the process, pressure variations in the distillation process, and holdup of dendritic feedstock for KAERI's ingot consolidation device. An in-depth description of these failure modes is expanded in this section.

The failure mode of poorly characterized feedstock in the distillation process is a result of the difficulty with determining the associated composition of the cathode

product. This can have several implications. The entrained salt is the greatest cause of these implications. It has been found that at the conditions associated with distillation that $PuCl_3$ can react with the U metal and cause Pu metal to remain in the final product ingot [26]. This presence of creates difficulties in taking accurate measurements of a consolidated ingot for safeguard measurements. In addition, presence of zirconium in the cathode product, which has the potential to be transported in the electrorefiner, could change the form the dendrites take when scraped and placed into the process crucible thus causing difficulties with distillation. Improper distillation will lead to the presence of salt, which contains active products which will cause problems for mass tracking and safeguard measurements for the same reasons stated before as Pu is present.

Poorly characterized feedstock occurs in the ingot fabrication process as a result of uncertainty on the cathode product and whether or not salt is still present in the cathode product after distillation. The composition of the dendritic product can affect the homogeneity and melting point as this is composition-dependent and materials of different density can lead to heterogeneity. Entrained salt will remain in a heterogeneous ingot. The active species present in the salt in the heterogeneous ingot again will cause problems for safeguards measurements.

Temperature variations in the salt distillation process can occur due to a partial or complete failure of the heating mechanism, in these cases an induction coil, as well as broken thermocouples. This is important to note as the temperature of distillation is critical to the CP's operation. At a temperature lower then what may be needed to distill off the salt in the dendrites will lead to salt being left entrained in the dendrites before it is melted into an ingot that results in a heterogeneous ingot.

Temperature variations in the ingot consolidation and melting furnace can fail due to failure of heating elements or loss of power just like the ER or distillation process. If the heating element is to fail, the high temperature required to melt and consolidate the ingot will extremely difficult to achieve. This could lead to a heterogeneous ingot, which has the same implications discussed previously.

Pressure variations in the distillation process can occur as a result of the failure of the vacuum pump or the air seal keeping the atmospheric gas out. This is important as the nominal pressure of the distillation process is 100 Pa to produce the separation of vapor pressures necessary for distillation [26]. This can lead to incomplete distillation, which produces the same challenges associated with heterogeneity discussed before.

The final failure mode only applies to the KAERI design and this is the failure of the feedstock delivery holdup mechanism. The feedstock delivery mechanism delivers dendrites continuously to the melting crucible of the ingot consolidator. The dendrites are delivered through an orifice that leads the mechanism into the melting crucible. This orifice has the potential to become jammed or congested thus restricting the delivery of dendrites. This would thus reduce the amount of dendrites being melted and thus reduce the mass of the U product ingots. This reduced product ingot would in turn lead to a smaller mass registered for the purpose of material accountancy thus having important safeguards implications as the mass registered would be less than the input disturbing the material balance.

3. MODELS

The modeling of the various signatures was performed in this work through the weak coupling of two different computer codes. The first was a code called Enhanced REFIN with Anodic Dissolution (ERAD) [28, 29, 30] that modeled the ER. The second code that it was coupled to was a MCNPx model of a non destructive assay instrument known as a JCC-31 High Level Neutron Coincidence Counter (HLNCC) [18]. This chapter describes the theory and computational background of these specific models.

3.1 ERAD

ERAD is a one dimensional computer code that models the electrorefiner in pyroprocessing. This model assumes that there is uniform potential at the cathode, anode, and homogenous salt bath. ERAD allows for the variation of several different inputs. These inputs include the composition of the anode and salt bath, the elements to be transported, and the operating parameters such as current, electrode surface area, time steps of operation. By utilizing these input parameters, ERAD calculates, for the inputted operation of the electrorefiner, the current for each element, the electrode potential, and the composition of the salt, anode, and cathode in terms of weight percentage and total mass of each element.

ERAD solves for these values through the use of three major calculations. The first of these calculations is the Nernst equation, which solves for the equilibrium potential of each element. The Nernst equation is seen in equation 2[29, 30]:

$$E_{eq,j} = E_j^o - \frac{RT}{n_j F} \ln\left(\frac{a_{b,j}^{red}}{a_{b,j}^{ox}}\right) \quad , \qquad (2)$$

where $E_{eq,j}$ is the equilibrium potential, E_j^o is the standard reduction potential of species j, R is the universal gas constant, T is the cell temperature, n_j is the number of electrons transferred for the reaction of species j, F is Faraday's constant, and $a_{b,j}^{red}$ and $a_{b,j}^{ox}$ are the activities of the reduced and oxidized form of species j respectively in the salt.

The second equation that ERAD solves is the Butler-Volmer equation, which calculates the rate at which a given element will be oxide or reduced. The Butler Volmer equation is seen in equation 3[29, 30],

$$I_j = i_{o,j}^o \left(a_{b,j}^{red}\right)^{\alpha_j} \left(a_{b,j}^{ox}\right)^{1-\alpha_j} \cdot A \left[\frac{a_{s,j}^{ox}}{a_{b,j}^{ox}} e^{\frac{\alpha_j n_j F}{RT}\eta_j} - \frac{a_{s,j}^{red}}{a_{b,j}^{red}} e^{-\frac{\left(1-\alpha_j\right)n_j F}{RT}\eta_j}\right], \quad (3)$$

where I_j is the current of species j, i_o^o is the standard exchange current density, α is the transfer coefficient, A is the electrode surface area, and η is the activation overpotential.

The final major calculation is the solution of the Nernst-Plank equation to calculate the mass transfer rate of each nuclide in the ER. The Nernst-Plank equation is seen in equation 4[29, 30],

$$\frac{\partial y_i}{\partial t} = -D_i \frac{\partial^2 y_i}{\partial x^2} - \frac{FD_i n_i}{RT} \frac{\partial}{\partial x} y_i \frac{\partial \Phi}{\partial x}, \quad (4)$$

where y is concentration in mol/cm^3, inside all diffusion layers, D is the diffusion coefficient in the electrolyte, n is the charge of the ion, R is the gas constant, T is absolute temperature, F is Faraday's constant, x is position, and $\frac{\partial \Phi}{\partial x}$ is the potential gradient. For more information on ERAD and its theory see the references [28, 29, 30]. ERAD was compiled and run on a Windows 8 operating system using the open source compiler "g95". A sample of an ERAD script is provided in Appendix A.

3.2 NDA MODEL

For the purpose of determining radiation signatures, a model was developed of the JCC-31 HLNCC in several iterations of the Monte Carlo N-particle Code (MCNP). The JCC-31 is a neutron coincidence counter developed by Los Alamos and distributed by Canberra [18]. The JCC-31 consists of a cylindrical sample chamber with an air environment surrounded by a polyethylene moderator. Within the polyethylene moderator are embedded 18 separate He-3 detectors. The sample chamber walls and the detector walls are lined with a thin layer of cadmium to shield from background and to prevent moderated neutrons from returning to the sample chamber and inducing fissions in the sample. The sample for analysis in the case of this work is the metallic fuel ingot consolidated from the dendrites of the metal transported in the ER. This ingot is placed at the center of the sample chamber and is counts a passive source of neutrons. A plot of the JCC-31 from the MCNP plotter is seen in Figure 5.

The He-3 tubes passively register these counts in a coincidence circuit. In a coincidence circuit, a neutron absorbed in any of the He-3 tubes is registered starting a predelay. In the case of the JCC-31, the predelay is 4 microseconds. After this pre-delay ends, a time gate of 64 microseconds is opened, and the total number of neutrons are counted. If only one neutron enters during this time gate then a single count is registered, if two neutrons enter a doubles count is registered as well as two singles counts. This leads to the determination of two separate rates of interest: the singles rate and the doubles rate.

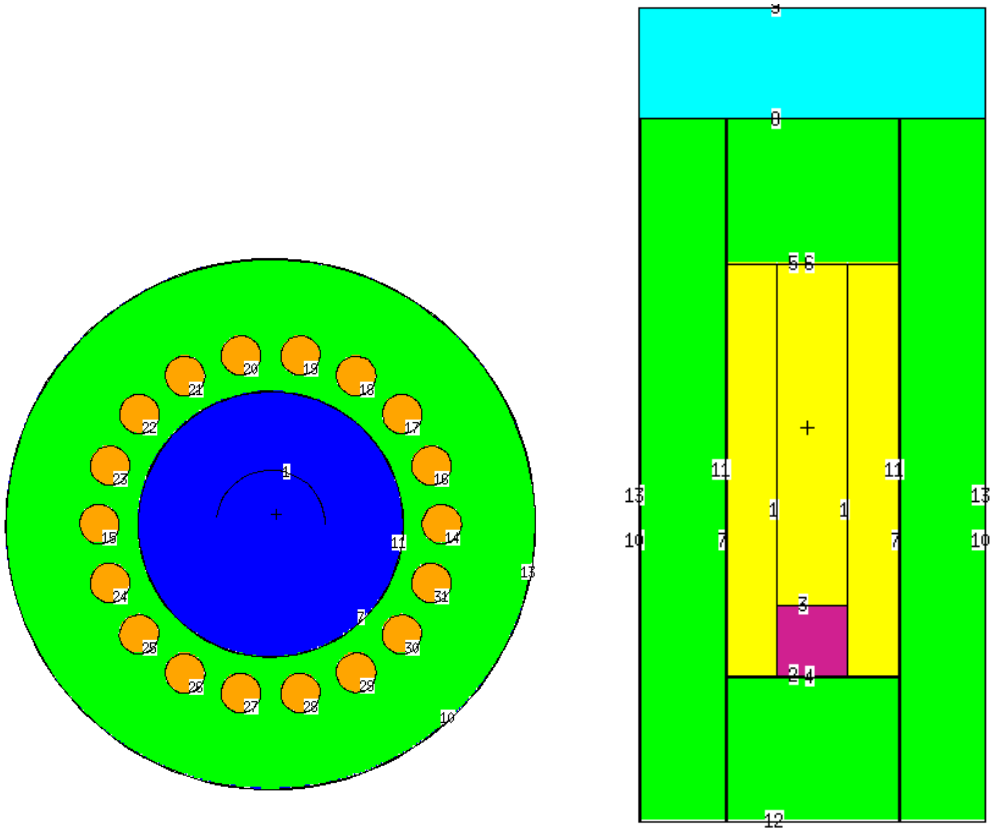

Figure 5- Top Down and Axial Cross Sections of JCC-31 HLNCC

These coincidence counts, as they are commonly called, can be simulated in MCNPx using the ft8 CAP tally [31]. This tally allows for the specification of the given predelay and time gate. These simulations for the determination of the coincidence count rates were performed on an Intel i7 processor with a Windows 8 operating system.

4. Modeling and Simulation Methodology

To determine equipment sensors and radiation signatures through computer modeling, a loose coupling of the two previously described codes was performed. These codes were coupled by taking the output of the ERAD model and inputting it in the MCNP detector model. This chapter describes how these two were coupled using burnup data. In addition, this chapter describes the particular studies performed to determine radiation signatures in terms of the different inputs and outputs of both ERAD and the detector model.

4.1. Coupling Overview

The coupling of the two codes was dependent on the type of failure mode being analyzed. There were two different basic methodologies that are similar in that they each have five steps but are different in terms of key inputs. The first methodology was for the case of ER failure modes and the second was for failures in the CP.

The methodology for failure modes in the ER involved five major steps. The first step was changing the input of ERAD to represent the failure mode of interest. After the input was changed, ERAD was run to calculate the compositions and potentials of the electrodes and salt. The cathode composition, which is in terms of elemental weight percentage, was converted into a composition of isotopic weight percentages for each element. This conversion was performed by applying weight percentages from a run of ORIGEN-ARP for 45000 MWd/MTIHM in a PWR for a 3 year cycle with 25 years cooling time [32]. This assumes that the isotopic weight percentages stay constant

throughout pyroprocessing, the only thing that changes and needs to be tracked is the elemental. These isotopic weight percentages were inputted into a homogenous cylindrical ingot at the center of the sample chamber of the JCC-31 model in MCNP. The code is then run with the homogeneous ingot outputting both singles and doubles counts from which their rates can be derived. A flow sheet of this methodology is seen in Figure 6.

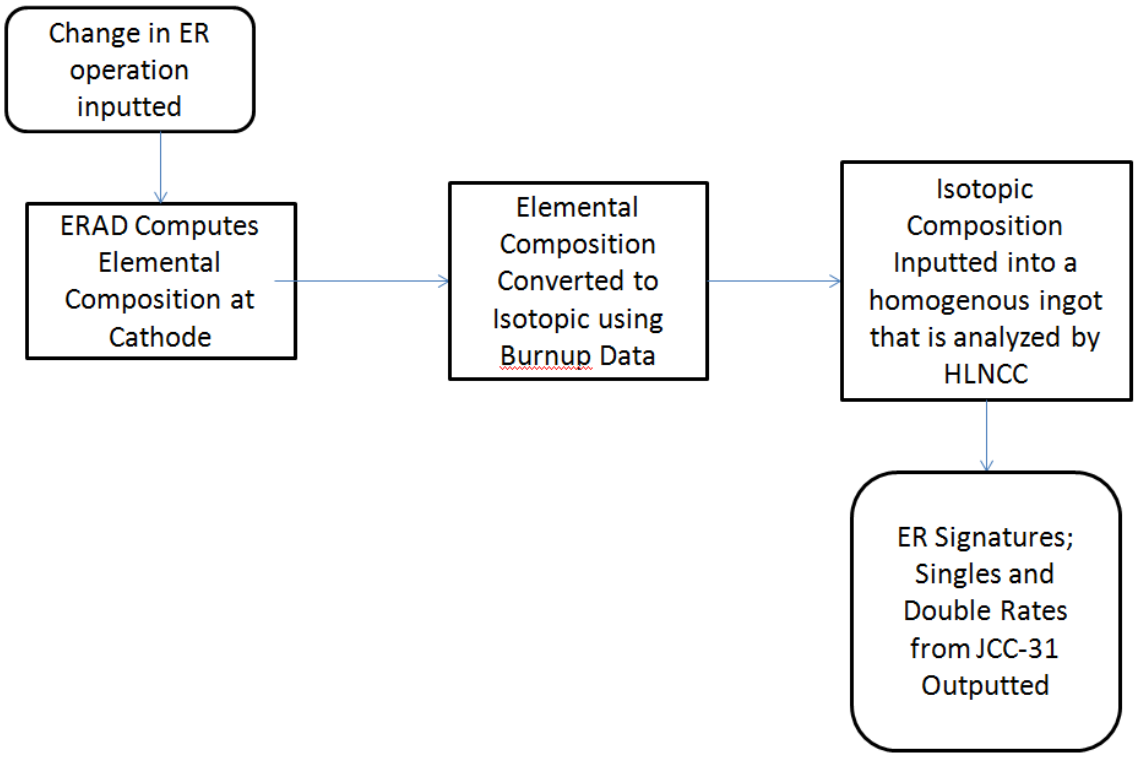

Figure 6- ER Failure Modes SBS Analysis Methodology Flow sheet

For the cathode processor failure modes a similar methodology was used. First the inputs into ERAD were changed to perform transport that would only allow uranium deposition at the cathode. ERAD was then run to calculate the composition and potential at the cathode and in the salt. The salt composition and the cathode composition were

then analyzed using the same burnup data as the ER study to convert the actinides in the cathodic product and salt to isotopic composition. The salt eutectic elemental weight percentages were converted to isotopic composition using the natural isotope atomic percentages from data from the *Chart of the Nuclides* [33]. Using these isotopic compositions a heterogeneous ingot was formed. This ingot consisted of two cylindrical layers. The first layer was the cathodic product and the second layer was the salt left entrained. The cathodic product layer was directly below the salt layer. This heterogeneous ingot was then analyzed by the JCC-31 in MCNP for singles and doubles counts from which their respective rates could be derived. This methodology is seen in Figure 7.

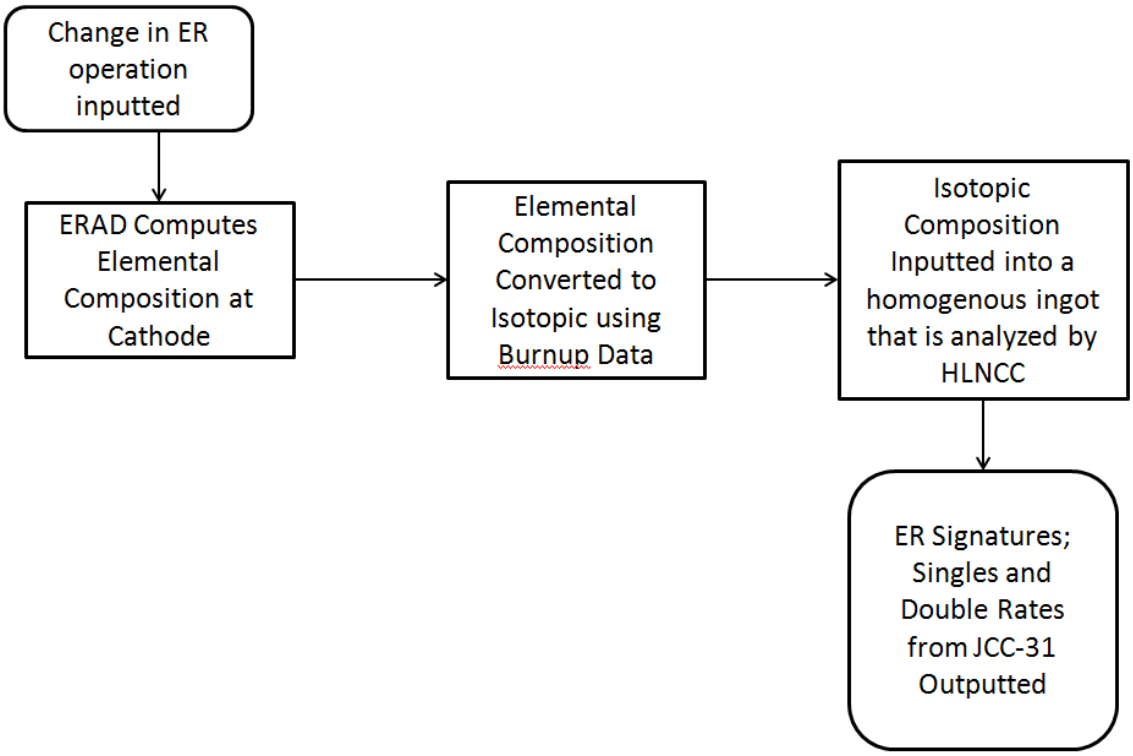

Figure 7- CP Failure Modes SBS Analysis Methodology Flow sheet

Details of the specific inputs and burnup data for these studies are documented in the subsequent sections.

4.2 ERAD METHODOLOGY

The inputs of ERAD differed depending on the failure mode to be analyzed. The failure modes analyzed were the poorly characterized anodic feedstock, reduction in cathodic surface area due to jamming of equipment, change in current due to electrical shorting, and change in diffusion layer thickness due to change in rotational speed of the electrode. The first three of these failure modes were analyzed using their own dedicated ERAD input test matrix. The change in electrode rotation speed and thus diffusion layer thickness had its own test matrix. The test matrix of inputs for the first three failure modes is seen in Table 3.

Table 3- Test Matrix for Poorly Characterized Anodic Feedstock, Reduced Electrode Surface Area, and Change in Current

Run	Applied Current (A)	Cathode Area (cm^2)	Current Density (A/cm^2)	Initial Pu/U salt mole ratio
i-1	72	800	0.090	0.030705
i-2	72	300	0.240	0.030705
i-3	72	150	0.480	0.030705
i-4	11.5	800	0.0144	0.14827
i-5	11.5	300	0.0383	0.14827
i-6	11.5	150	0.0767	0.14827
i-7	85	800	0.106	0.336838
i-8	85	300	0.283	0.336838
i-9	85	150	0.567	0.336838
i-10	30	800	0.0375	1.62658
i-11	30	300	0.100	1.62658
i-12	30	150	0.200	1.62658

As demonstrated in the Table, there are 12 different runs over four different groups of currents and initial Pu/U ratio. By comparing results within a group, one can see the effect of changing cathode surface area and thus current density. By comparing between the four groups, one can see the impact of initial salt composition and changes in currents on overall mass transported and its effects in off normal scenarios.

The test matrix developed for the changes in the diffusion layer thickness due to changes in electrode rotation speed are seen in Table 4. These values were taken from a CFD study in the open literature for electrorefiner modeling [24]. As can be seen the study demonstrates the affects of the change of diffusion layer thickness primarily but also allows for the demonstration of the effects of current density and salt composition changes as well.

Table 4- Test Matrix for Study of the Variation of Diffusion Layer Thickness

Run	Applied Current Density (A/cm^2)	Diffusion Layer Thickness, δ (μm)	Initial Pu/U salt mole ratio
δ-1	0.125	200	0.337
δ-2	0.125	210	0.337
δ-3	0.125	220	0.337
δ-4	0.125	230	0.337
δ-5	0.125	240	0.337
δ-6	0.0275	150	1.627
δ-7	0.0275	200	1.627
δ-8	0.0275	250	1.627
δ-9	0.0275	300	1.627
δ-10	0.0275	350	1.627

For the final case of the cathode processing failure modes, the test matrix was simply runs i-1, i-4, i-7, and i-10 from Table 4. This is because the primary concern is not the contents of the ingot; it is the composition of the salt, which will be inputted into the final

ingot. Thus the only thing to vary is the initial mass of entrained salt, which is altered in its own test matrix governed by the input of the MCNP analysis.

4.3 Conversion of Elemental Composition to Isotopic Composition

As stated in the coupling overview, the elemental composition in terms of weight percent was converted to isotopic weight percentages for the purpose of input into the MCNP model of the HLNCC. This was performed by multiplying the elemental weight percentages by the isotopic weight percentages and coding it in MCNP as one homogenous ingot or heterogeneous ingot with salt layer depending on the failure mode analyzed. The data from the ORIGEN-ARP run for this conversion is seen in Table 5.

Table 5- Uranium and Plutonium Isotopic Compositions Calculated in ORIGEN for Input into Detector Model

Uranium Isotope	Weight Fraction		Plutonium Isotope	Weight Fraction
U232	2.504E-09		PU236	1.95E-12
U233	1.91E-08		PU237	0.00E+00
U234	3.65E-04		PU238	3.48E-02
U235	9.02E-03		PU239	6.399E-01
U236	6.42E-03		PU240	1.82E-01
U237	2.00E-11		PU241	2.25E-02
U238	9.84E-01		PU242	1.21E-01
U239	0.00E+00		PU243	4.56E-17
			PU244	1.3E-05

4.4 MCNP Model Methodology

After the isotopic composition was determined, the ingot could be programmed into MCNP for the purpose of being analyzed by the simulated detector. The entries into MCNP for the geometry, materials, and sources of each run differed depending on the type of failure mode being analyzed.

For ER failure modes, the ingot analyzed was that of a homogenous metal ingot with the composition representative of the cathodic product with no salt left entrained. The ingot was modeled as a cylinder whose height was twice that of the diameter. The exact volume could be determined by using equation 5 to solve for the density and the dividing the total mass by the density.

$$\rho_{mix} = \frac{1}{\sum \frac{x_j}{\rho_j}}, \tag{5}$$

where x_j and ρ_j are the mass fraction and density of species j, respectively. The source for the ER failure modes was dependent on the composition of the ingot and was calculated by hand using data from the *Chart of the Nuclides*.

The source for ER failure modes was modeled as being spontaneous fission as there were no low atomic mass elements to produce alpha-n reactions. ER detector analyses were analyzed using MCNPx-POLIMI for their advanced specific spontaneous fission sources [34]. MCNPx-POLIMI allows for specification of isotopes of spontaneous fission and this specification defines the source term. The isotopes specified in the case of the ER failure modes were the U-238 and Pu-240 isotopes and the source was evenly distributed probabilistically over the entire ingot. By calculating the source strength, the

amount of fissions from a given nuclide can also be determined and the fraction of the total source from these two specific isotopes for the ER analyses can be computed. This fraction and these specific fractions were inputted into the specialized source terms allowing for the computation. The total number of spontaneous fissions divided by the number of source fissions provides the total counting time. This total counting time is important as it provides the basis for the count rate when dividing the tally results by the total time of counting. The number of these source fissions runs differed to produce low MCNP tally uncertainties.

The ingot for the case of the CP failure modes was modeled as a two layered heterogeneous ingot, one of the metallic cathode product and one of the salt left entrained. The metallic portion followed the same geometry guidelines as the ER ingot for the metallic cathodic product in that it was a cylinder of twice the height as the diameter. The salt layer then was the same diameter, but its height differed depending on the weight percentage of salt left entrained. The test matrix of the CP failure modes involved analyzing this weight percentage for 0.1, 0.5, 1.0, 3.0, and 5.0 weight percent of salt entrained. An example of an MCNP script for the ER failure modes is seen in Appendix B.

The source term of the CP failure separated ingot was evenly distributed over the salt layer. This was because the metallic product was entirely uranium and thus not very active comparatively to the entrained salt that contained both alpha-n neutron reactions that produced a neutron source and spontaneous fission neutrons. The script was programmed for use in MCNP6. This was due to its newly released status at the time and its updated data and multiprocessing capabilities. To simulate the source of neutrons from

the salt two separate MCNP scripts were developed. The first script handled neutron sources that came from alpha-n neutron reactions while the second handled neutrons coming from spontaneous fissions. This source was determined by using the software SOURCES-4C developed by Texas A&M in conjunction with Los Alamos National Labs [35]. SOURCES-4C requires the composition and concentration of the actinides and low mass nuclides that will produce alpha-n reactions to be inputted. Running SOURCES-4C with the calculated composition and concentrations from ERAD and the burnup data, the code calculated the probabilistic energy distribution and both alpha-n neutron and spontaneous fission source rates. The spontaneous fission script was generated by placing the command "PAR=SF" in the source definition portion of the MCNP script. The alpha-n script was generated by inputting the calculated probabilistic energy distribution using an ERG card. These two scripts were run for the time required for 1 million source spontaneous fissions to occur. Thus, the alpha-n source script always required more source particles than the spontaneous fissions as more alpha-n neutrons were emitted per second than there were source spontaneous fissions. An example of the alpha-n source script is seen in Appendix C. An example of the spontaneous fission source MCNP script is seen in Appendix D.

The MCNP tallies in each case used were ft8 CAP tallies [31]. These tallies simulate coincidence counting and allow for the calculation of singles and doubles counts and its rates. The detector was also assumed to be properly shielded from background thus making so all counts registered come from the ingot itself. For the case of the CP failure modes, the rates from both the spontaneous fission and alpha-n script were added to calculate the total rates. The ER failure modes just involved the results of their

particular script. In the calculation of each script, the estimated detector uncertainty of the result calculated was reflect an actual detector as the capture tally involved completely analog Monte Carlo with no variance reduction. In the case of the CP failure modes, the total uncertainty of the combined sum involved propagating the uncertainty from the results of both scripts. The squares of each total uncertainty were added and a square root was taken [36]. This provided the total uncertainty of the combined rate.

4.5 TREATMENT OF CURIUM

Neutron measurements of spent fuel for mass determination and other safeguards purposes are normally dominated by the presence of Cm-244, an isotope that is a strong source of spontaneous fission neutrons. It has been often assumed that curium and plutonium track each other throughout the pyroprocessing system with a constant ratio of masses [37]. The tracking of curium counts has been proposed as a method for safeguarding nuclear material for this reason. The rationale for this is the assumptions made in relation to their thermodynamic and electrochemical properties. The most relevant property being the Gibb's free energy which is -64 kcal/mol for $CmCl_3$ and -62.4 kcal/mol for $PuCl_3$[38]. The standard reduction potentials differ however, thus demonstrating that there should be a certain level of segregation of the two species occurring in electrochemical cells such as the electrorefiner. Still, even if the segregation occurs, the Cm-244 present in a final product will be the dominant source of neutron making it impossible to produce an accurate mass determination measurement for plutonium.

To address these issues with the presence of curium, a method known as Residual Actinide Recovery (RAR) has been developed by KAERI [12]. This process involves adding $CdCl_2$ to the salt in the ER to re-oxidize the curium and remove it from the final product as seen by the chemical equation in equation 6:

$$3CdCl_2 + 2Cm \leftrightarrow 3Cd + 2CmCl_3 \quad (6)$$

This process will also oxidize plutonium and uranium that has attached itself to the cathode, but the effect should be minimal comparatively to that of the curium. Any electrochemical unit operation not employing this process would most likely result in deposition of curium and thus produce a neutron source that is nearly 100% Cm-244 in a pure metallic ingot. For the purpose of this study, the process was assumed to be employed and was used to remove curium from any final metallic product analyzed thus only even uranium and plutonium isotopes could contribute to the source. For salt entrained studies however, such as the CP failure modes, the salt was assumed to maintain the ratio of curium to plutonium derived from the burnup data of .00308.

For an anomalous scenario identification method such as SBS this removal of curium may cause unnecessary difficulties. The presence of curium would produce a strong neutron source that could be detected with little difficulty by any neutron detector used to analyze it. By removing the curium, this advantage in detecting an anomalous scenario would be lost. Thus, if SBS is to be implemented in the future in an actual facility, then removal of actinides will most likely not want to be performed as to lose this significant advantage. However, the analyses in this thesis are for the much more challenging case to detect in which RAR is applied.

5. Results of ER Failure Mode Analyses

Results from both ERAD and the MCNP model were determined to indicate signatures for SBS as applied to pyroprocessing. This chapter consists of three sections. The first discusses the results and analyses of signatures seen from ERAD. The second presents the results and analyses of the results determined by the MCNP detector model for the radiation signatures from the final metallic product[39, 40]. The last section provides a short discussion of the detector uncertainty derived from the MCNP model and its implications with regards to SBS.

5.1 Results from ERAD

5.1.1 Current Density and Salt Composition Study Results

The results for the first test matrix where changes were made to the current density and initial concentrations of plutonium and uranium are seen in Table 6. As can be seen, the current density and the cathode surface area can vary significantly before it exceeds the limiting current density and leads to the deposition of plutonium. Thus, a significant jamming of the electrode would be needed for this deposition to occur. In addition, as expected, with increased current, the mass of total material deposited increases. Finally, with a higher initial ratio of Pu/U, we see that the quantity of plutonium deposited comparatively to the uranium deposited increases significantly. This illustrates the continuing importance of ensuring that the salt in the electrorefiner has been treated to remove active products during periods of operation and these actinides being placed in their own dedicated waste form as illustrated in the previous flow sheet.

Table 6- Current Density Test Matrix (Table 3) Results for Cathodic Deposition from ERAD

Run	Current Density (A/cm^2)	Initial Pu/U salt mole ratio	U Mass Deposited (g)	Pu Mass Deposited (g)	Total Mass Deposited (g)
i-1	0.090	0.030705	5120	1.00E-07	5120
i-2	0.240	0.030705	5120	1.00E-07	5120
i-3	0.480	0.030705	5020	98.3	5118.3
i-4	0.0144	0.14827	817	1.00E-07	817
i-5	0.0383	0.14827	817	1.00E-07	817
i-6	0.0767	0.14827	765	52.6	817.6
i-7	0.106	0.336838	6040	1.00E-07	6040
i-8	0.283	0.336838	6040	1.00E-07	6040
i-9	0.567	0.336838	5440	608	6040
i-10	0.0375	1.62658	2130	1.00E-07	2130
i-11	0.100	1.62658	2060	74.6	2130
i-12	0.200	1.62658	1170	970	2130

The effect of cathode surface area on cathode potential is seen in Figure 8. As can be seen, the potential increases in the case of a reduced surface area where transport of plutonium occurs. In addition, a change in surface area of any kind produces a change in potential. This can be used as a potential signature to be integrated into a SBS framework through the use of a reference electrode in the ER to measure the potential.

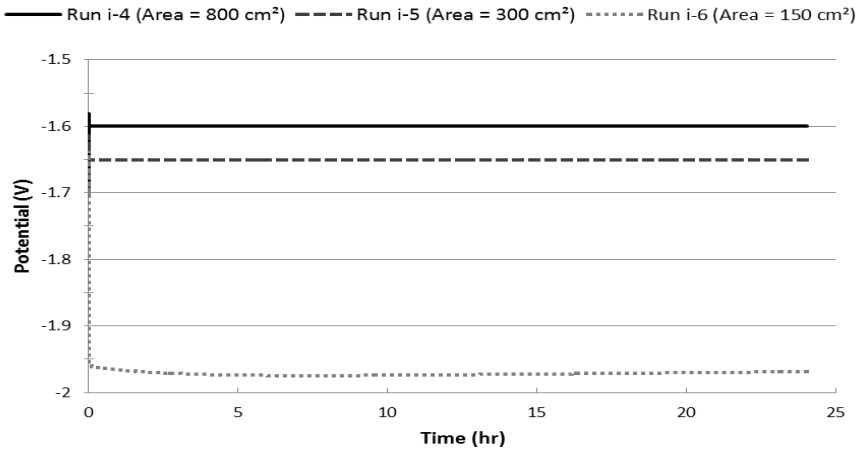

Figure 8- Effect of Cathode Surface Area on the Cathode Potential Profile

5.1.2 Diffusion Layer Thickness Study Results

The results of the second test matrix for the diffusion layer thickness study are seen in Table 7. As demonstrated by the table, only slight variations in the diffusion layer thickness are required for plutonium transport to occur in the ER. Thus, ensuring that the ER is operating at the prescribed electrode rotation speed is important. If it is not operating at the correct speed, then the deposition of plutonium will most likely raise an alarm in a SBS framework indicating diversion that may be difficult for a safeguards agency such as the IAEA to diagnose.

Table 7- Diffusion Layer Thickness Test Matrix (Table II) Results for Cathodic Deposition from ERAD

Run	Applied Current Density (A/cm^2)	Diffusion Layer Thickness, δ (μm)	Initial Pu/U salt mole ratio	U Mass Deposited (g)	Pu Mass Deposited (g)
δ-1	0.125	200	0.337	7104.5	0.0
δ-2	0.125	210	0.337	6737.6	370.3
δ-3	0.125	220	0.337	6510.6	599.2
δ-4	0.125	230	0.337	6278.9	832.8
δ-5	0.125	240	0.337	6070.0	1043.4
δ-6	0.0275	150	1.627	1563.1	0.0
δ-7	0.0275	200	1.627	1397.9	166.5
δ-8	0.0275	250	1.627	1145.6	420.9
δ-9	0.0275	300	1.627	978.7	589.2
δ-10	0.0275	350	1.627	855.3	713.6

The effect of change in diffusion layer thickness on the cathode potential is seen in Figure 9. Like with the changes in surface area, there is an increased negative potential with an increase in diffusion layer thickness. However, for small perturbations in diffusion layer thickness, the change in potential is not significantly large even though the amount of plutonium deposited is. Thus, integrating this signal into SBS and being able

to determine that this failure mode has occurred will be more challenging than determining that the failure mode has occurred for the signal from change in cathode surface area due to the need to define what a standard acceptable operating range of potentials is for an ER.

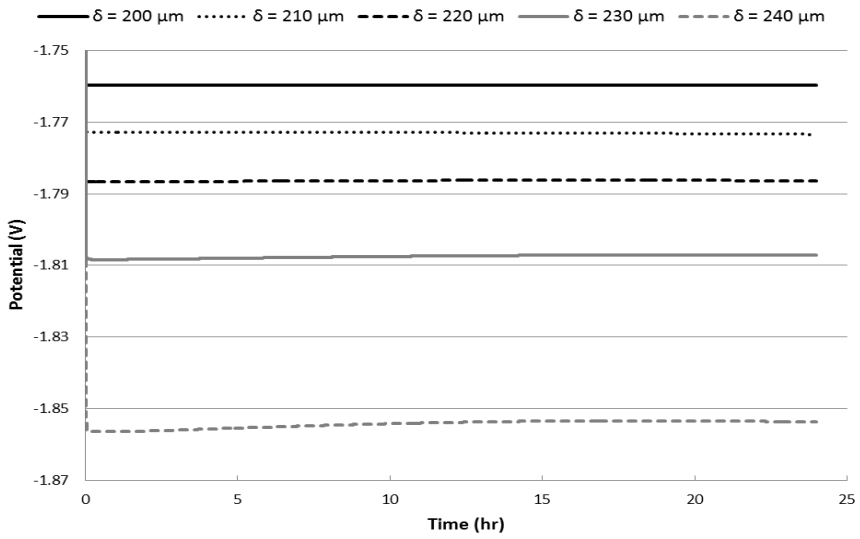

Figure 9- Effect of diffusion layer thickness on cathode potential

5.2 Results from Detector Model

5.2.1 Current Density and Salt Composition Study Results

Using the results for the first test matrix for changes in current density and initial concentration in the salt, the spontaneous fission rate and individual contribution from a given element could be calculated. The results of these calculations are seen in Table 8.

Table 8- Contribution of Uranium and Plutonium to the Overall Spontaneous Fission Rates for Current Density Test Matrix (Table 3)

Run	% Contribution by U	% Contribution by Pu	Fission Rate (sec^{-1})	Total Number of Source Fissions
i-1 & i-2	100	0	34.5	2.00E+07
i-3	0.4	99.6	8600.9	3.00E+07
i-4 & i-5	100	0	5.5	3.00E+07
i-6	0.1	99.9	4589.4	4.00E+06
i-7 & i-8	100	0	40.66	1.00E+08
i-9	0.7	99.3	53026	1.00E+07
i-10	100	0	14.3	3.00E+07
i-11	0.2	99.8	6515.5	3.00E+07
i-12	0	100	84634	1.00E+06

By dividing the total number of source fissions by the fission rate, the total counting time can be determined. By dividing the total counts by this total counting time, the count rates can be determined. As demonstrated by the results, with increased plutonium content there is an increased source of neutrons that is proportional to the total mass deposited. This is expected due to the spontaneous fissions that occur from Pu-240, which are significantly greater in total emission rate than the U-238 spontaneous fissions neutrons.

The results from the detector model for the given rates with uncertainties are seen in Table 9. A plot of the contribution of mass of plutonium to singles and doubles rates is seen in Figures 10 and 11. The uncertainties are plotted on the figures however the values are so small that they are not visible. These low uncertainties illustrate that the model has reached a conclusive results. As fully analog capture was used, these uncertainties also are representative of the actual detector uncertainties of the detector.

Table 9- MCNPx Results for Current Density Test Matrix (Table 3)

Run	U Mass deposited (g)	Pu Mass deposited (g)	Singles Rate ± Uncertainty (cps)	Doubles Rate ± Uncertainty (cps)
i-1 & i-2	5120	1.00E-07	0.876 ± 0.0012	0.0466 ± 0.00029
i-3	5020	98.3	279 ± 0.279	20.3 ± 0.079
i-4 & i-5	817	1.00E-07	0.119 ± 0.00015	0.00514 ± 0.000031
i-6	765	52.6	128 ± 0.40	7.91 ± 0.0989
i-7 & i-8	6040	1.00E-07	1.05 ± 0.0006	0.0577 ± 0.00016
i-9	5440	608	2010 ± 3.4	189 ± 1.1
i-10	2130	1.00E-07	0.336 ± 0.00071	0.016 ± 0.00016
i-11	2060	74.6	195 ± 0.37	12.8 ± 0.095
i-12	1170	970	3960 ± 19	544 ± 7.5

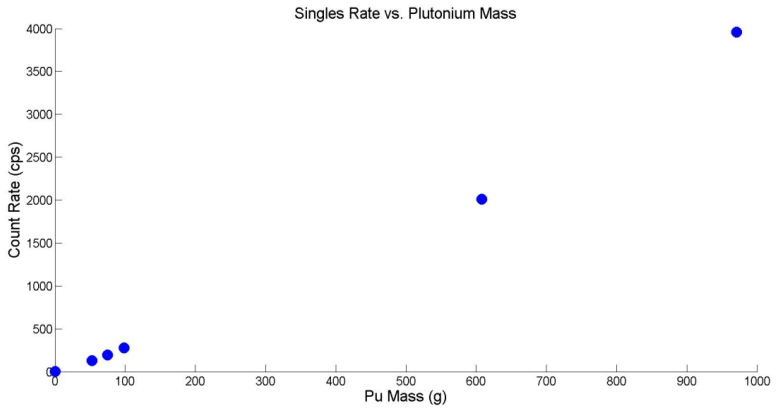

Figure 10- Singles Rate vs. Plutonium Mass Deposited For Current Density Test Matrix as Shown in Table 9

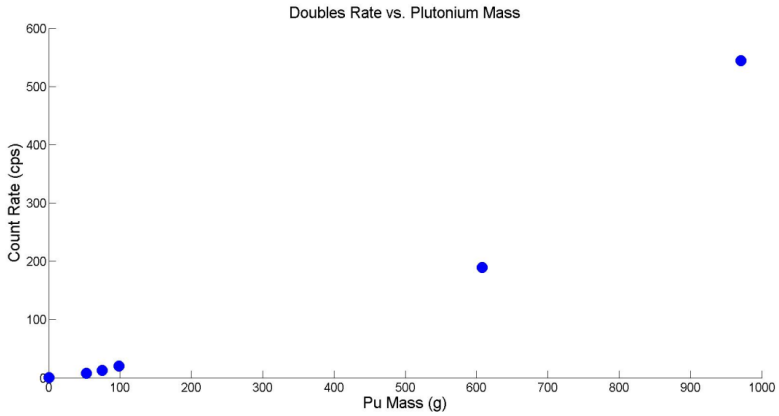

Figure 11- Doubles rate vs. Plutonium Mass Deposited For Current Density Test Matrix as Shown in Table 9

Inspecting the data from the tables and figures demonstrates the profound impact that the presence of plutonium has with regards to overall count rate for the detector. With increased plutonium deposition, an increased count rate is seen due to increased mass of Pu-240 and thus an increase in neutron source. For both singles and doubles rates, a minor deposit of plutonium leads to a significantly larger count rate than the product that features essentially no plutonium as is the case of normal operation. Most importantly, the doubles rate is highly distinguishable from the pure uranium case in all cases that involve plutonium deposition. These two count rates can both serve as significant signatures for an SBS type application. In addition, the figures demonstrate that there is a linear relationship between plutonium mass deposited and the counts registered. In reality, at higher count rates, this relationship would most likely be linear and the actual registered count rate would be less due to the presence of detector dead time. Detector dead time was not factored into the analyses carried out in this modeling work. However, even if dead time was present, the issue of counts as being applied as a signature would not change as they would still show a significant difference than in the case of the pure uranium product.

Of the upmost importance for signature identification in SBS, is determining the signatures associated with specific events or failures. For this type of analysis, the results of single and double count rates versus current density are seen in Figures 12 and 13. These results correspond with the failure modes seen in the test matrix in Table 3. As shown in both figures 12 and 13, the rates increase quadratically with increasing current density. It stays as a low count value, until it reaches a level above the limiting current density for a given composition thus leading to an abrupt jump in counts due to

deposition of plutonium. This shows that current density can change and still produce no plutonium transport and subsequently counts. This is especially true for cases that involve low currents or lower plutonium to uranium ratios. However, at higher plutonium to uranium ratios it is demonstrated that the change in current density and thus surface area is smaller and thus more sensitive to set off an alarm. Various scenarios could lead to a higher Pu/U ratio in the salt, including errors in the addition of oxidant, uranium drawdown, or differing used fuel compositions. In all of these cases, the HLNCC demonstrates that it can detect changes in actinide content that are a result of changes in current density. These results demonstrate the potential ability of these signals to be integrated into an SBS framework and effectively detect and diagnose these off normal scenarios.

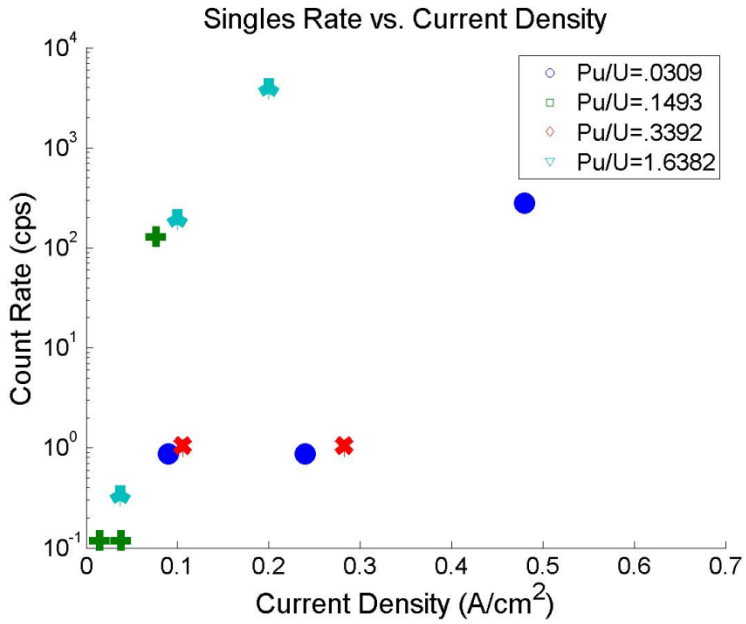

Figure 12- Singles Rate vs. Current Density (Legend: circle -- Pu/U = 0.0309, + -- Pu/U = 0.1493, x -- Pu/U = 0.3392, Three Pronged Symbol -- Pu/U = 1.6382)

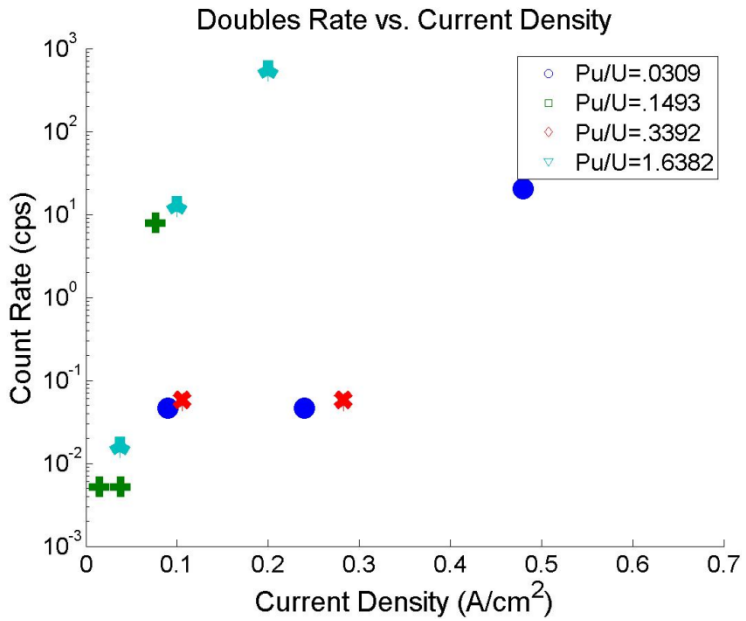

Figure 13- Doubles Rate vs. Current Density (Legend: circle -- Pu/U = 0.0309, + -- Pu/U = 0.1493, x -- Pu/U = 0.3392, Three Pronged Symbol -- Pu/U = 1.6382)

5.2.2 Diffusion Layer Thickness Study Results

Using the results for the first test matrix for changes in cathode diffusion layer thickness, the spontaneous fission rate and individual contribution from a given nuclide could be calculated. The results of these calculations are seen in Table 10. Again it is demonstrated that with increased plutonium deposition there is an increased source strength that is proportional to the total mass deposited.

Table 10- Contribution of Uranium and Plutonium to the Overall Spontaneous Fission Rates for Diffusion Layer Thickness Test Matrix (Table 4)

Run	% Contribution by U Fissions	% Contribution by Pu Fissions	Fission Rate (sec^{-1})	Number of Source Fissions
δ-1	100	0	6	2.00E+07
δ-2	0.1	99.9	32318	4.00E+06
δ-3	0	100	52266	1.00E+06
δ-4	0	100	72623	1.00E+06
δ-5	0	100	90976	1.00E+06
δ-6	100	0	10.5	2.00E+07
δ-7	0.1	99.9	14520	4.00E+06
δ-8	0	100	36664	1.00E+06
δ-9	0	100	51357	1.00E+06
δ-10	0	100	62198	1.00E+06

The detector response modeled by MCNP for these cathodic products are shown in Table 11 and Figures 14 and 15.

Table 11- MCNPx Results for Cathode Diffusion Layer Thickness Text Matrix (Table 4)

Run	Applied Current Density (A/cm^2)	δ(μm)	Initial Pu/U salt mole ratio	Singles Rate ± Uncertainty (cps)	Doubles Rate ± Uncertainty (cps)
δ-1	0.125	200	0.337	1.26 ± 0.0018	0.071 ±0.0004
δ-2	0.125	210	0.337	1161 ± 3.1	98.5 ± 0.95
δ-3	0.125	220	0.337	1966 ± 11	179 ± 3.26
δ-4	0.125	230	0.337	2909 ± 15	296 ± 4.94
δ-5	0.125	240	0.337	3844 ± 20	432 ± 6.78
δ-6	0.0275	150	1.627	0.239 ± 0.00036	0.0217 ±0.00015
δ-7	0.0275	200	1.627	451 ± 1.3	33 ± 0.36
δ-8	0.0275	250	1.627	1331 ± 7.3	128 ± 2.32
δ-9	0.0275	300	1.627	2060 ± 11	227 ± 3.70
δ-10	0.0275	350	1.627	2712 ± 14	677 ± 10.0

The change in the singles count rates is linearly proportional to the thickness of the cathode diffusion layer. At higher current densities, the slope of this line is greater. Thus in a commercial facility where current is expected to be high as to maximize transport and throughput, only a slight increase in diffusion layer thickness due to a reduced rotational speed could generate a singles rate that could potentially set off an alarm in an SBS integrated system. The doubles rate follows a more quadratic relationship between count rate and diffusion layer thickness. The doubles rate is important as they are reflective of the fissile material present and are not as sensitive to background. Thus, doubles rates have great significance as signatures in ER product analysis. The doubles rates at lower current densities will be harder to detect for slight changes as the effect on doubles count rates due to changes in diffusion layer thicknesses is lower at lower diffusion layer thicknesses. However, at higher current densities, the coincidence counter can be used as an effective tool for detecting signatures of off normal operations.

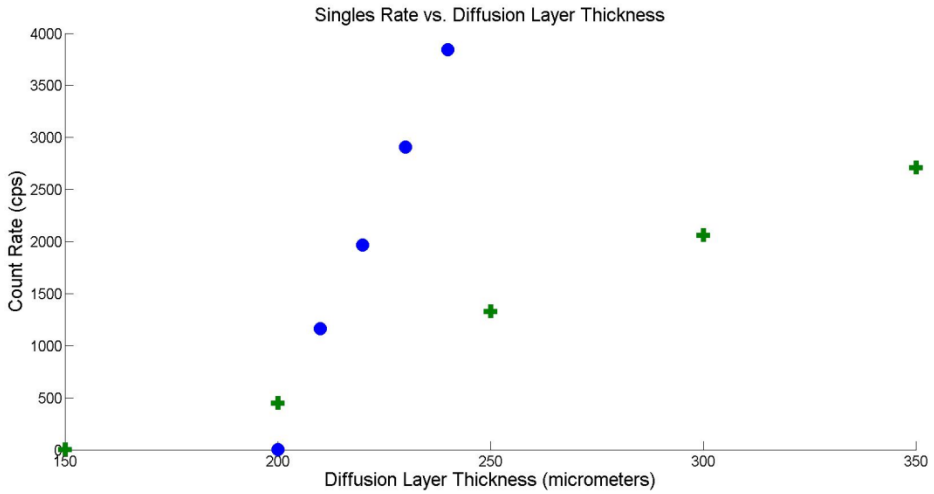

Figure 14- Singles Rate vs. Diffusion Layer Thickness (Legend: Circle -- Applied Current Density = 0.125 A/cm2, + -- Applied Current Density = 0.0275 A/cm2)

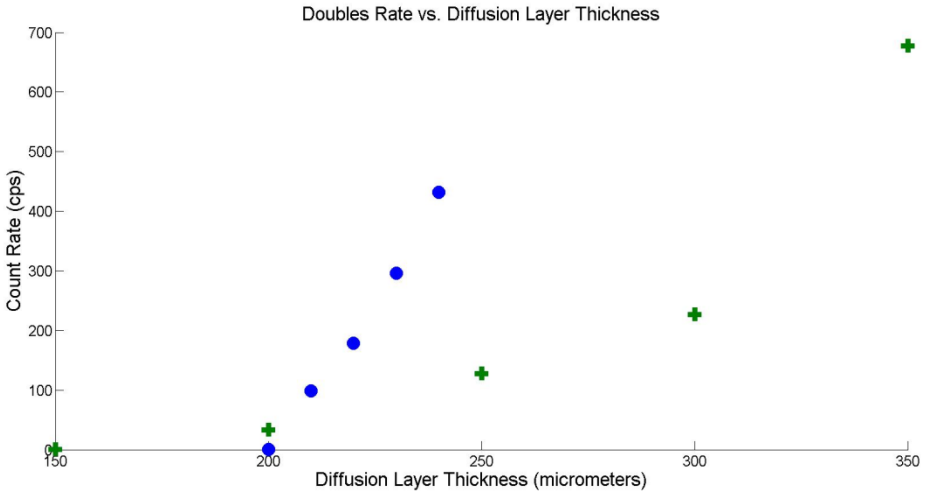

Figure 15- Doubles Rate vs. Diffusion Layer Thickness (Legend: Circle -- Applied Current Density = 0.125 A/cm2, + -- Applied Current Density = 0.0275 A/cm2)

5.3 MEASUREMENT UNCERTAINTY ANALYSES

One of the greatest challenges with applying the knowledge obtained from computer modeling analyses such as these with a real application is the presence of measurement uncertainties in the counts of the neutron detector. The counts from the model will be significantly less than that obtained by detectors in a real system. This is due to multiple reasons. The first is that the measurement uncertainties of detector counts are equal to the square root of the total counts. Counts are proportional to the time that the detector is allowed to count the neutrons provided by the ingot. As the number of source fissions in these analyses is great, the total counting time is also great especially in the case of the pure uranium product cases where the counting times are on the scales of hours, days or even weeks. The counting times in an actual pyroprocessing facility due to the need for high throughputs will posses shorter counting times and thus a higher

measurement uncertainties for no to low plutonium deposition and thus making the signal for SBS harder to distinguish as to being within the acceptable range or not. As no counting times have been determined, an estimate of the quantity of detector uncertainty of a measurement in an actual facility has yet to be determined. This time however can be determined through the use of system models of what an efficient pyroprocessing facilities timing scheme looks like. In addition, this quantification can be aided with information from the PRIDE facility relating to material throughput and unit operation time. By scaling up this information, one can determine how much time can possibly be spent on a given counting measurement without affecting the overall throughput of the facility.

6. Results of Cathode Processor Failure Modes

In addition to failure modes for the ER, failure modes for the CP were analyzed for potential signatures to be integrated into an SBS framework. This chapter describes first the ERAD and SOURCES-4C results and second the results obtained from the MCNP analysis for the developed test matrix[41].

6.1 ERAD and SOURCES-4C Results

The study in ERAD for the CP failure modes involved using runs 1, 4, 7, and 10 from the current density text matrix as they were representative of circumstances where the ER operated without the presence of any failure mode. This would result in the deposition of only uranium at the cathode. The results of these runs as well as the results for the source strength of these compositions from SOURCES-4C are shown in Table 12. It was found that after one 12 hour operation of the ER that the change in composition of the ER salt was negligible. Thus, the listed initial weight percentages are also the end of operation weight percentages. This is important to note, as it emphasizes the importance of constant monitoring of signals and processes as the saturation of the salt with actinides will require time and continual operation.

Table 12- Calculated Source from SOURCES-4C

Case #	U wt% in Salt	Pu wt% in Salt	U Cathode Mass	Alpha-n Source (n/cm^3-s)	SF Source (n/cm^3-s)
1	7.57	0.234	5120	29.27	2.998
4	1.57	0.234	817	30.5	2.997
7	7.57	2.57	6040	329.2	32.92
10	1.57	2.57	2130	331.2	32.92

6.2 MCNP MODEL RESULTS

The results of the MCNP detector model for singles and doubles rates versus weight percentage of salt left entrained in the ingot is seen in Figures 16 and 17. In both cases there is a linear relationship between weight percentage of salt entrained and the count rate registered. In addition, there was a greater ratio of singles rate to doubles rate compared to results seen for cases for the ER failure modes. This is due to the primary neutron source within the detector being due to alpha-n reactions, which do not emit multiple neutrons, do not induce as many fissions, and the neutrons released are of a lower energy. The lower energy neutrons emitted are absorbed more often in the cadmium liner, which is a strong absorber of epithermal neutrons.

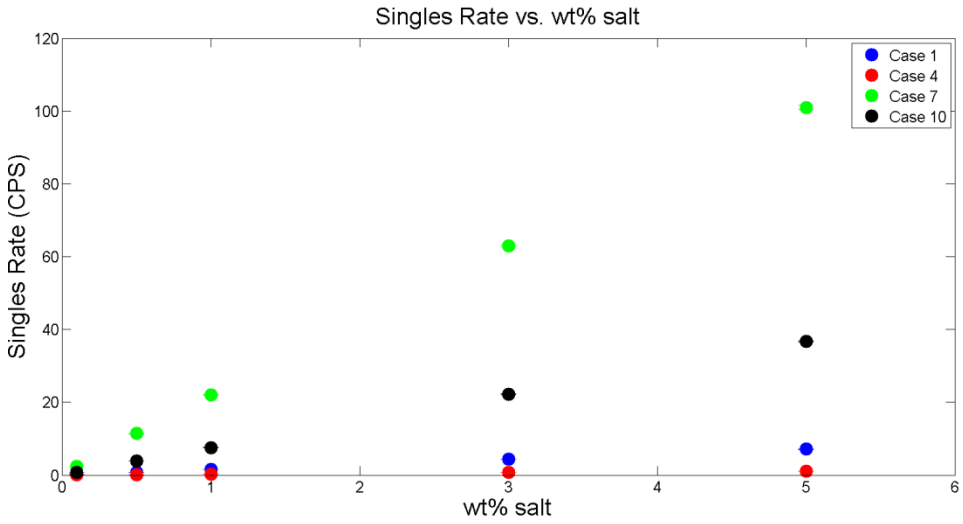

Figure 16- Result of MCNP6 Coincidence Counting Tallies for Singles Rate for CP Failure Modes

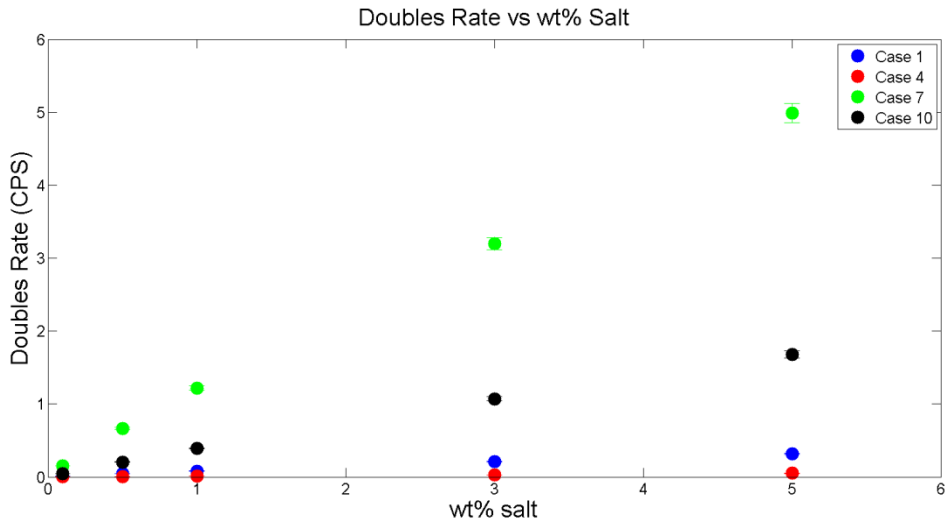

Figure 17- Result of MCNP6 Coincidence Counting Tallies for Doubles Rate for CP Failure Modes

Comparing between the different cases, the salts with the higher weight percentage of plutonium, case 7 and 10, are significantly greater in terms of produced count rate than those with less. This is due to the greater number of spontaneous fissions and alpha-n reactions as a result of the increased plutonium and the curium content , which are much more active species than uranium. This produces a greater source of neutrons and thus more neutrons to be counted in a given period of time. Also, comparing between cases of the same weight percentages of plutonium, the ingots that have the most uranium mass register the highest counts as this provides the greatest mass of salt entrained and thus greatest source. In addition, greater uranium mass also means that there is more fissile material that the source from the salt can induce fissions in.

Examining the error bars, there is a greater error in the results of the case of higher weight percentages for the same number of source fissions and alpha-n source neutrons. These error bars represent the measurement uncertainty of the detector. This

increased measurement uncertainty is due to there being a fewer fission in the uranium ingot because the salt layer is larger and thus the distance to travel between salt layer and ingot is increased. For this reason, fewer counts occur over a given number of source particles run. However, as the count rates are significantly higher, in an actual counting situation the time required to attain a low uncertainty measurement would be less. Thus in an actual safeguards measurement, these counts would be registered with lower uncertainties and thus be more conclusive signatures.

The results of these simulations demonstrate that signatures do exist for counting measurements of ingots with salt entrained. However, for low plutonium content, we see a significantly lower count rate especially at lower weight percentages of total salt entrained. In addition, the doubles rate is especially low and would be difficult to register to obtain a high confidence rate to be utilized for a signature for any weight percentage of salt entrained. The singles rate could still potentially be a signature. For this reason, though it was applicable as an instrument for registering counting signatures for ER failure modes, the JCC-31 may not be the most applicable NDA tool for the purposes of identifying signatures for integration into an SBS framework as it may not be able to sufficiently monitor all failure modes that affect the final ingot. Thus, other NDA techniques and devices should be investigated in the future to determine if there are ones that are more effective for this purpose and can either be used in conjunction with the JCC-31 or be a replacement for use in an SBS system. This future investigation could involve additional neutron detection methods or gamma measurements. The JCC-31, despite this, if coupled with high confidence measurements like density measurements and visual inspection could still be effective as a signature identification tool.

7. SUMMARY AND CONCLUSIONS

NMA face several challenges when applied to reprocessing. Electrochemical reprocessing or pyroprocessing in particular faces many challenges using NMA due to the lack of an upfront input accountability tank and inconvenient and unrealistic plant flushouts. Thus, alternate methods for safeguarding pyroprocessing using PM to aid and decrease the uncertainty of normal NMA measurements are being investigated. One PM method of particular interest with demonstrated efficacy is the Signature Based Safeguards (SBS) approach. SBS involves determining signatures that indicate that off normal operations are occurring and integrating data from sensors within a pyroprocessing facility to raise an alarm if anomalous operations are occurring. This allows detection to occur in real time and not just at the end of cycle NMA audit.

One challenge faced in safeguarding pyroprocessing is failure modes within plant operations that would appear to be malicious diversions. Work to determine signatures that indicate these failure modes is important to successfully operating and safeguarding an advanced fuel cycle facility. The work undertaken for this thesis involved identifying failure modes and investigating their signatures.

The first step in performing this was determining failure modes for the ER and CP process equipment. These failure modes then needed to be simulated to determine signatures that would arise. This was done by coupling an ER model in a computer code known as ERAD and an NDA instrument known as the JCC-31 HLNCC in MCNP. To couple the two, the failure modes for the ER were simulated in ERAD by changing their

inputs. After simulating these failure modes, the output of ERAD was consolidated into an ingot that was analyzed for both singles and double coincidence rates in MCNP.

A qualitative analysis of the results simulated in the modeled analyses are tabulated in Table 13 for a given failure mode with respect to their overall safeguards significance and potential detectability by the sensors within a SBS framework. Each failure mode is ranked as to both their significance and detectability being high, medium, or low. The safeguards significance reflects the failure modes to produce a loss of COK. The detectability reflects the amount that the results diverge from the normal operating state and the number of sensors that can detect it.

Table 13- Qualitative Summary of Failure Mode's Safeguard Significance and Detectability (Ranked: H-High, M-Medium, L-Low)

Failure Mode Identified	Safeguard Significance	Detectability
ER Failure Modes		
Poorly Characterized Anodic Feedstock	L	L
Change in Electrode Submersion Depth	M	M
Change in Electrode Rotational Speed	H	H
CP Failure Modes		
Poorly Characterized CP Feedstock	M	L
Temperature Variation of CP	L	M
Pressure Variation of CP	L	M

The conclusions of the ER failure modes demonstrate that there is a certain level of hierarchy with regards to the safeguards significance of a failure mode. Poorly characterized anodic feedstock is of low safeguards significance due to it not being the primary reason for the deposition of material in the cathode that could produce a safeguard relevant scenario. It only decides the ratio of uranium to plutonium in the combined metal. The safeguard significance of the change in electrode submersion depth is ranked as medium as it contributes directly to the deposition of plutonium at the cathode; however, there is a significant operational range under, which deposition will not occur even though it is not operating as designed. The significance of the electrode rotational speed is classified as high due to the deposition of plutonium of occurring with only slight changes in diffusion layer thickness and thus small changes in rotational speed thus causing a potential loss of COK. The detectability of the poorly characterized feedstock is low as there are no corroborating sensors along with a radiation detector that can indicate that the feedstock possesses a certain level of safeguards significance. The detectability of change in submersion depth is classified as medium as sensors of the both the reference electrode and radiation detector can only detect and determine it in the cases in , which the submersion depth changes significantly enough to deposit plutonium. Only a sensor determining electrode depth would be able to notice the failure mode if it does not result in deposition. Finally, the detectability of the change in rotational speed is high as the sensors, RPM meter, reference electrode, and radiation detector all can realize and detect the slight changes that lead to deposition when outputs are combined together.

For the CP failure modes, the safeguard significance of poorly characterized CP feedstock is categorized as medium. This is due to it being the deciding factor as to the

amount of plutonium that can remain if a failure mode occurs or plutonium chloride reacts with uranium. The failure modes of temperature variation and pressure variation are labeled as low safeguards significance, as the failure has to be significant enough to generate a large amount of residual salt or else the amount of plutonium that remains is very low and of little interest from a COK perspective. The detectability of poorly characterized feedstock is labeled as low as the radiation detector outputs are low and this is the only way of seeing that a failure mode has occurred in this fashion. The detectability of the mode of temperature and pressure variations are labeled as medium, as, even though the radiation detector is not a very good sensor for detecting this anomaly, the other sensors such as pressure gauges and thermocouples will most likely be able to detect a change in operating conditions.

LIST OF APPENDICES

APPENDIX A- SAMPLE ERAD SCRIPT

```
Stage 1 - Continuous electrorefining, uranium extraction: RB -
02.11.2009
&input1
  !Temperature (keep at 773 Kelvin unless other parameters are
changed accordingly)
    temp=773.d0,
  !Number of elements being tracked in the system
    nelemt=10,
  !Elemtn names (not used, but useful in remembering)
    ename = 'Ur', 'Pu', 'Nd', 'Cd', 'Li', 'Ka', 'Cl', 'Np', 'Na',
'Zr',
  !Standard potentials for each elements (Reverse of conventional
sign)
  !  stde  = 2.501d0, 2.76d0, 0.36d0, 0.635d0, 3.683d0, 3.865d0,
-0.895d0, 9.68d0,9.5d0,2.2,
    stde  = 1.113d0, 1.372d0, 0.36d0, 0.635d0, 3.683d0, 3.865d0,
-0.895d0, 9.68d0,9.5d0,0.81,
  !taken from CV paper and from (zr needs updated)
  !Diffusion coefficients in liquid cadmium
    diffu1= 1.51d-5, 1.0d-5,  1.5d-9, 1.5d-5, 1.5d-5, 1.5d-5,
1.5d-5, 1.5d-9, 1.5d-9,1.d-5,
  !Estimated
  !Diffusion coefficients in molten salt
    diffu2= 2.E-05, 8d-5, 1d-5, 2.23d-5, 1.13d-5, 2.5d-5, 2.5d-5,
1d-9, 1d-9, 1.5d-5,
  !Taken from cv paper and from australian paper
  !Standard exchange current densities (A/cm^2)
    curr0 = 1E-00, 0.8, 5d-9, 5d-9, 5d-9, 5d-9, 5d-9, 5d-9, 5d-9,
.8d-0
  !Taken from cv paper and zr guessed
  !Species valance states
    zi    = 3.000d0, 3.0d0, 3.0d0, 2.00d0, 1.0d0, 1.0d0, -1.0d0,
3.0d0,1.0d0,4.0d0,  !X!
  !Transfer coefficient for anode (alpha)
    tca   = 5.0E-01, 0.5d0, 0.5d0, 0.50d0, 0.5d0, 0.5d0,
0.5d0,0.5d0,0.5d0,0.5d0,   !X!
  !Transfer coefficient for cathode (alpha)
    tcc   = 5.0E-01, 0.5d0, 0.5d0, 0.5d0, 0.5d0, 0.5d0,  0.5d0,
0.5d0, 0.5d0, 0.5d0, !X!
  !initial cathode potential (Volts) [-0.5 to -3.0]
    catp=-2.7d0, !X!
  !initial anode potential  (Volts) [-0.5 to -3.0]
    anop=-2.5d0, !X!
  !Number of current 'steps';
    ipset=1, !x!
  !End time of current 'steps' (hours)
```

```
    tset= 6.02  !X!
  !Current setting for each current 'step' (Amps)
    cmaxt= 0.4d0 !X!
  !Absolute error for Butler-Volmer Solver (recomended: less than
1d-16)
    aberr=1.d-15,
  !Solubility limit for elements in Cadmium pool (mole fraction)
    psolim =  0.0113d-2, 0.018d-2, 1.0d0, 1.0d0, 1.0d0, 1.0d0,
1.0d0, 1.0d0, 1.0d0, 0.00295d-2
  !Cyclic voltammogram option: tmodi = 'cyclic'
  !  tmodi = 'cyclic'
  !CV scan rate (V/s) sign of number indicates starting direction
  !  sr = -.1
  !Cv start voltage, maximum voltage, and minimum voltage
  !  v = -1.000, -1.35, -1.8
  !Output coordinate for first column on tables (mnemonic X
select) 1=coulombs passed, 2=time in seconds, 3=time in hours
    xsel = 1
  !Period between major outputs such as (plots of diffusion
layers) unit selected by xsel
     outperiod = 100.
  !Supress CV output before tcrit
     osupress = .False.
  !Add column headings to output
     colheading = .TRUE.
  !.TRUE.=Write cathode contents to restart file/ .FALSE. Write
original cathode contents to restart file
     writecathode = .TRUE.
  !Used to specify plot monitor of bulk compositions and
concentrations 0=Off
     plotmonitorcon = 1
  !Used to specify to display plot monitor of surface plots 0=Off
     plotmonitorsurf = 0
  !used to specify which elements to monitor on the monitor plot.
For all element, input " ", example: 'Ur Pu Zr'
!    plotelelist = ' '
     plotelelist=" Ur Pu Zr"
/
&sanode
!Type of solid anode (3=cylinder, 2=cylinder with clad)
  sflag = 003,
!Number of cells in Zr region
  nzr = 40,
!Initial mesh cell size in Zr region
  dy2o=1.0d-7,
!Radius of fuel segement
  r0 = 0.2855d0, !X! Assumed
!Height of fuel segement
  hi0 = 2.640d0,  !X! With mass and volume and density
assumptions
!Number of chopped fuel segements
  ncfs = 1,
```

```
!Fraction of electrolyte diffusion coefficient in Zr region due
to porous media (normally a guess)
  dfrac = .031000d0
!Set initialize to 90232 if you want to skip it
  initialize = 90232
  slimcon = -00.1
/
&input2
!Size of anodic liquid metal diffusion layer [keep it the size of
1*dy in this code version] (cm)
  del(1)=1.0E-03,
!Size of anodic molten salt diffusion layer (cm)
  del(2)=15.0E-03
!Size of cathodic molten salt diffusion layer (cm)
  del(3)=20.0E-03
!Size of cathodic liquid metal diffusion layer [set to 1*dy if
solid cathode] (cm)
  del(4)=1.0E-03
!Mesh Size (cm)
    dy=1.0E-03,
!Contact area of anode-salt, cathode-salt, and pool-salt
interfaces (cm^2)
  area= 4.73, 45.23d0 !x!
/
&INPUT3
!Solver settings.  Don't mess with them unless you edit the
source code.
  ISTATE=1,
  ITASK=5,
  epslon=1.d-5
  iopt=1,
!Maximum number of computations per timestep.  (Has never helped
the result)
  mxstep=100,
!First timestep size (seconds).  Keep it small
  h0=1d-15
!Keep this set to 5, which tells lsoda to compute a banded
jacobian.
  jt=5,
!Matrix lower bandwidth.  Its minimum value seems to be 19 when
using 10 elements.
!Smaller=faster bigger->more stable
!Smaller->faster bigger->more stable
  ml=99,
!Matrix upper bandwidth.  Its minimum value seems to be 19 when
using 10 elements.
  mu=99,
!Maximum timestep
  hmax=50.0d0
  itol=1,
!LSODA/E relative tolerance (I have found it best to keep this
number less than 10d-20, but feel
```

```
!free to play with it)
  rtoli=1.d-22
!LSODA/E absolute tolerance (This will likely need adjusting.  I
have found it should be less than
!1d-6, and preferably beween 1d-10 and 1d-8.  With lsoda, running
smaller that 1d-12 causes the code
!to crash.  With lsode, I have not found a lower limit, but would
still reccomend keeping the tolerance
!above 1d-12 for the sake of speed
  atoli=1.d-13
  iprint=2,
/
&input4
!Composition of anode (weight fraction)
 Can= 70d-2, 20d-2, 1.0d-9, 1.0d-9, 1.0d-9, 1.0d-9, 1.0d-9, 1.0d-
9, 1.0d-19, 10d-2, !X!
!Composition of electrolyte (weight fraction)
 Cms= 00.73d-2, 3.10d-2, 1.d-9, 1.d-9, 6.87d-2, 2.78d-1, 6.18d-1,
1d-9, 1d-19, 0.003d-2, !X!
!Composition of cathode (weight fraction)
 Cca=  1d-7, 1d-7, 1d-9, 1d-9, 1d-9, 1d-9, 1d-9, 1d-9, 1d-19, 1d-
9, !X!
!Composition of pool (weight fraction)
 Cpo=  1d-3, 1d-3, 1d-9, .98d-0, 1d-9, 1d-9, 1d-9, 1d-9, 1d-9,
1d-9,
!Composition of pool intermetallics (weight fraction)
 Cim=  9d-3, 5d-3, 1d-9, 8d-3, 1d-9, 1d-9, 1d-9, 1d-9, 1d-9, 1d-
9,
!Composition of inlet stream (weight fraction)
 Cin=  1.5d-11, 1.0d-11, 1.d-11, 1.d-11, 7.368d-2, 28.842d-2,
63.789-2, 1d-11, 1.52d-11, 1d-11,
/
&input5
!masses of anode, electrolyte, cathode, pool, and pool
precipitate (g)
  mass= 9.6d0, 1065d0, 1.0d-2, .6, .2  !X!
!
! if vol specified, volume is used
! if dens specified, volume is calculated via density
  dens = 14.2, 1.7813 , -7.8148, 1, 1
! density taken from zr density paper in archives
  vol = -0.9295d0, -97.87d0,0.01d0, -42,-1
!Atomic weights of the elements
  gatom=238.03,  240.0, 144.24, 112.41, 6.939, 39.1, 35.453,
237.0d0,22.9d0,91.224d0 !x!
/
```

APPENDIX B- SAMPLE MCNPX-POLIMI SCRIPT FOR ER FAILURE MODES

```
Model JCC-31 for High Level Neutron Coincidence Counting
c ******************************
c Cell Cards
c ******************************
100  1000 -19.1  -1 2 -3 imp:n=1 $Uranium Ingot
110  2000 -8.65   -2 4 -7 imp:n=1 $Cadmium SHield
120  3000 -.0013   -1 -5 3 imp:n=1 $ Surrounding Air In Sample
Compartment
130  3000 -.0013   1 -7 2 -5  imp:n=1$ Surrounding Air In Sample
Compartment
140  2000 -8.65    -7 5 -6 imp:n=1 $ Cadmium Shield
150  4000 -0.92    6 -8 -7 imp:n=1 $Poly Reflector
160  5000 8.636e-2 -13 8 -9 imp:n=1 $Stainless Steel Electronics
170  2000 -8.65    7 -11 12 -8 imp:n=1 $Cadmium Shield
180  4000 -0.92    -7 -4 12 imp:n=1 $Poly Reflector
190  4000 -0.92    11 -10 12 -8 14 15 16 17 18 19 20 21
                   22 23 24 25 26 27 28 29 30 31 imp:n=1 $Poly
Reflector
314  4000 -0.92    32 -8 -14 imp:n=1    $Poly Reflector
315  4000 -0.92    32 -8 -15 imp:n=1    $Poly Reflector
316  4000 -0.92    32 -8 -16 imp:n=1    $Poly Reflector
317  4000 -0.92    32 -8 -17 imp:n=1    $Poly Reflector
318  4000 -0.92    32 -8 -18 imp:n=1    $Poly Reflector
319  4000 -0.92    32 -8 -19 imp:n=1    $Poly Reflector
320  4000 -0.92    32 -8 -20 imp:n=1    $Poly Reflector
321  4000 -0.92    32 -8 -21 imp:n=1    $Poly Reflector
322  4000 -0.92    32 -8 -22 imp:n=1    $Poly Reflector
323  4000 -0.92    32 -8 -23 imp:n=1    $Poly Reflector
324  4000 -0.92    32 -8 -24 imp:n=1    $Poly Reflector
325  4000 -0.92    32 -8 -25 imp:n=1    $Poly Reflector
326  4000 -0.92    32 -8 -26 imp:n=1    $Poly Reflector
327  4000 -0.92    32 -8 -27 imp:n=1    $Poly Reflector
328  4000 -0.92    32 -8 -28 imp:n=1    $Poly Reflector
329  4000 -0.92    32 -8 -29 imp:n=1    $Poly Reflector
330  4000 -0.92    32 -8 -30 imp:n=1    $Poly Reflector
331  4000 -0.92    32 -8 -31 imp:n=1    $Poly Reflector
200  2000 -8.65   -13 10 12  -8 imp:n=1 $Cadmium SHield
214  6000 -.0001785 -14 12 -32 imp:n=1  $He-3 Detector
215  6000 -.0001785 -15 12 -32 imp:n=1 $He-3 Detector
216  6000 -.0001785 -16 12 -32 imp:n=1  $He-3 Detector
217  6000 -.0001785 -17 12 -32 imp:n=1  $He-3 Detector
218  6000 -.0001785 -18 12 -32 imp:n=1  $He-3 Detector
219  6000 -.0001785 -19 12 -32 imp:n=1  $He-3 Detector
220  6000 -.0001785 -20 12 -32 imp:n=1  $He-3 Detector
221  6000 -.0001785 -21 12 -32 imp:n=1  $He-3 Detector
222  6000 -.0001785 -22 12 -32 imp:n=1  $He-3 Detector
223  6000 -.0001785 -23 12 -32 imp:n=1  $He-3 Detector
224  6000 -.0001785 -24 12 -32 imp:n=1  $He-3 Detector
225  6000 -.0001785 -25 12 -32 imp:n=1  $He-3 Detector
226  6000 -.0001785 -26 12 -32 imp:n=1  $He-3 Detector
```

```
227  6000 -.0001785 -27 12 -32 imp:n=1  $He-3 Detector
228  6000 -.0001785 -28 12 -32 imp:n=1  $He-3 Detector
229  6000 -.0001785 -29 12 -32 imp:n=1 $He-3 Detector
230  6000 -.0001785 -30 12 -32 imp:n=1  $He-3 Detector
231  6000 -.0001785 -31 12 -32 imp:n=1  $He-3 Detector
210  0             13:-12:9 imp:n=0 $Outside World

c ******************************
c Surface Cards Defining Detector
c ******************************
1 cz 2.811
2 pz 0
3 pz 11.242
4 pz -0.04
5 pz 40.6
6 pz 40.64
7 cz 8.5
8 pz 54.85
9 pz 65.85
10 cz 17
11 cz 8.54
12 pz  -14.25
13 cz 17.04
14 c/z 11 0 1.27
15 c/z -11 0 1.27
16 c/z 10.3366 3.7622 1.27
17 c/z 8.4625 7.0707 1.27
18 c/z 5.5 9.5263 1.27
19 c/z 1.910 10.8329 1.27
20 c/z -1.910 10.8329 1.27
21 c/z -5.5 9.5263 1.27
22 c/z -8.4265 7.0707 1.27
23 c/z -10.3366 3.7622 1.27
24 c/z -10.3366 -3.7622 1.27
25 c/z -8.4625 -7.0707 1.27
26 c/z -5.5 -9.5623 1.27
27 c/z  -1.9101 -10.8329 1.27
28 c/z 1.9101 -10.8329 1.27
29 c/z 5.5 -9.5263 1.27
30 c/z 8.4265  -7.0707 1.27
31 c/z 10.3366 -3.7622 1.27
32 pz 36.55

c ******************************
c Data Cards
c ******************************
c Source Definition
nps 2e7
sdef pos= 0.0 0.0 0.0 axs= 0. 0. 1 rad=d1 ext=d2  $ erg=d3
si1= 0.0 2.811
sp1= -21 1
si2= 0.0 11.242
```

```
sp2= 0 1
c si3= L 2 3 4 5 6 7
c sp3= 9.689e-11 6.6025e-5 1.15499e-6 .971065 2.39294e-2
4.93867e-3
IPOL 2 -1 1 1 0 0 18 214 215 216 217 218 219 220 221 222 223 224
225
       226 227 228 229 230 231
c ******************************
c Material Definition
c ******************************
m1000      92233     -1.92e-8           $ U/TRU Ingot
         92234     -3.65e-4
         92235     -9.02e-3
         92236     -6.425e-3
         92237     -6e-12
         92238     -.984
         94238     -6.5370e-13
         94239     -1.2009e-11
         94240     -3.4141e-12
         94241     -4.4236e-13
         94242     -2.2661e-12
         94243     -8.5542e-28
         94244     -2.439e-16
m2000    48106     .0125
         48108     .0089
         48110     .1249
         48111     .1280
         48112     .2413
         48113     .1222
         48114     .2873
         48116     .0749
m3000 7014.70c     0.8      8016.70c    0.2  $ air
m4000 1001.70c     2.0      6000.70c   1.0   $ polyethylene
mt4000     poly.10t
c STAINLESS-STEEL
c       Cr number density = 1.6540e-2
c       Fe number density = 6.3310e-2
c       Ni number density = 6.5100e-3
c    total number density = 8.6360e-2
c
c
m5000 24050  7.1866e-4     $ Cr-50  4.345%
      24052  1.3859e-2     $ Cr-52 83.789%
      24053  1.5715e-3     $ Cr-53  9.501%
      24054  3.9117e-4     $ Cr-54  2.365%
      26054  3.7005e-3     $ Fe-54  5.845%
      26056  5.8090e-2     $ Fe-56 91.754%
      26057  1.3415e-3     $ Fe-57  2.119%
      26058  1.7853e-4     $ Fe-58  0.282%
      28058  4.4318e-3     $ Ni-58 68.0769%
      28060  1.7071e-3     $ Ni-60 26.2231%
      28061  7.4207e-5     $ Ni-61  1.1399%
```

```
      28062  2.3661e-4     $ Ni-62  3.6345%
      28064  6.0256e-5     $ Ni-64  0.9256%
m6000 2003  1.0             $Helium 3
f8:n (214 215 216 217 218 219 220 221 222 223 224 225 226 227 228
      229 230 231)
c  fm4 1 6000 1
c  sd4 1
ft8:n cap 2003 gate 400 6400
```

APPENDIX C- SAMPLE MCNP6 SCRIPT FOR ALPHA-N NEUTRON SOURCE FOR CP FAILURE MODES

```
Model JCC-31 for High Level Neutron Coincidence Counting
c ******************************
c Cell Cards
c ******************************
100  1000 -19.1  -1 2 -3 imp:n=1 $Uranium Ingot
101  7000 -1.24  -1 3 -99 imp:n=1 $Salt Entrained
110  2000 -8.65   -2 4 -7 imp:n=1 $Cadmium SHield
120  3000 -.0013   -1 -5 99 imp:n=1 $ Surrounding Air In Sample
Compartment
130  3000 -.0013   1 -7 2 -5  imp:n=1$ Surrounding Air In Sample
Compartment
140  2000 -8.65    -7 5 -6 imp:n=1 $ Cadmium Shield
150  4000 -0.92    6 -8 -7 imp:n=1 $Poly Reflector
160  5000 8.636e-2 -13 8 -9 imp:n=1 $Stainless Steel Electronics
170  2000 -8.65    7 -11 12 -8 imp:n=1 $Cadmium Shield
180  4000 -0.92    -7 -4 12 imp:n=1 $Poly Reflector
190  4000 -0.92    11 -10 12 -8 14 15 16 17 18 19 20 21
                   22 23 24 25 26 27 28 29 30 31 imp:n=1 $Poly
Reflector
314  4000 -0.92    32 -8 -14 imp:n=1    $Poly Reflector
315  4000 -0.92    32 -8 -15 imp:n=1    $Poly Reflector
316  4000 -0.92    32 -8 -16 imp:n=1    $Poly Reflector
317  4000 -0.92    32 -8 -17 imp:n=1    $Poly Reflector
318  4000 -0.92    32 -8 -18 imp:n=1    $Poly Reflector
319  4000 -0.92    32 -8 -19 imp:n=1    $Poly Reflector
320  4000 -0.92    32 -8 -20 imp:n=1    $Poly Reflector
321  4000 -0.92    32 -8 -21 imp:n=1    $Poly Reflector
322  4000 -0.92    32 -8 -22 imp:n=1    $Poly Reflector
323  4000 -0.92    32 -8 -23 imp:n=1    $Poly Reflector
324  4000 -0.92    32 -8 -24 imp:n=1    $Poly Reflector
325  4000 -0.92    32 -8 -25 imp:n=1    $Poly Reflector
326  4000 -0.92    32 -8 -26 imp:n=1    $Poly Reflector
327  4000 -0.92    32 -8 -27 imp:n=1    $Poly Reflector
328  4000 -0.92    32 -8 -28 imp:n=1    $Poly Reflector
329  4000 -0.92    32 -8 -29 imp:n=1    $Poly Reflector
330  4000 -0.92    32 -8 -30 imp:n=1    $Poly Reflector
331  4000 -0.92    32 -8 -31 imp:n=1    $Poly Reflector
200  2000 -8.65   -13 10 12  -8 imp:n=1 $Cadmium SHield
214  6000 -.0001785 -14 12 -32 imp:n=1  $He-3 Detector
215  6000 -.0001785 -15 12 -32 imp:n=1 $He-3 Detector
216  6000 -.0001785 -16 12 -32 imp:n=1  $He-3 Detector
217  6000 -.0001785 -17 12 -32 imp:n=1  $He-3 Detector
218  6000 -.0001785 -18 12 -32 imp:n=1  $He-3 Detector
219  6000 -.0001785 -19 12 -32 imp:n=1  $He-3 Detector
220  6000 -.0001785 -20 12 -32 imp:n=1  $He-3 Detector
221  6000 -.0001785 -21 12 -32 imp:n=1  $He-3 Detector
222  6000 -.0001785 -22 12 -32 imp:n=1  $He-3 Detector
223  6000 -.0001785 -23 12 -32 imp:n=1  $He-3 Detector
224  6000 -.0001785 -24 12 -32 imp:n=1  $He-3 Detector
```

```
225  6000 -.0001785 -25 12 -32 imp:n=1  $He-3 Detector
226  6000 -.0001785 -26 12 -32 imp:n=1  $He-3 Detector
227  6000 -.0001785 -27 12 -32 imp:n=1  $He-3 Detector
228  6000 -.0001785 -28 12 -32 imp:n=1  $He-3 Detector
229  6000 -.0001785 -29 12 -32 imp:n=1 $He-3 Detector
230  6000 -.0001785 -30 12 -32 imp:n=1  $He-3 Detector
231  6000 -.0001785 -31 12 -32 imp:n=1  $He-3 Detector
210  0             13:-12:9 imp:n=0 $Outside World

c ******************************
c Surface Cards Defining Detector
c ******************************
1 cz 2.7734
2 pz 0
3 pz 11.0935
4 pz -0.04
5 pz 40.6
6 pz 40.64
7 cz 8.5
8 pz 54.85
9 pz 65.85
10 cz 17
11 cz 8.54
12 pz  -14.25
13 cz 17.04
14 c/z 11 0 1.27
15 c/z -11 0 1.27
16 c/z 10.3366 3.7622 1.27
17 c/z 8.4625 7.0707 1.27
18 c/z 5.5 9.5263 1.27
19 c/z 1.910 10.8329 1.27
20 c/z -1.910 10.8329 1.27
21 c/z -5.5 9.5263 1.27
22 c/z -8.4265 7.0707 1.27
23 c/z -10.3366 3.7622 1.27
24 c/z -10.3366 -3.7622 1.27
25 c/z -8.4625 -7.0707 1.27
26 c/z -5.5 -9.5623 1.27
27 c/z  -1.9101 -10.8329 1.27
28 c/z 1.9101 -10.8329 1.27
29 c/z 5.5 -9.5263 1.27
30 c/z 8.4265  -7.0707 1.27
31 c/z 10.3366 -3.7622 1.27
32 pz 36.55
99 pz 11.26455

c ******************************
c Data Cards
c ******************************
c Source Definition
mode n
nps 23626885
```

```
sdef pos= 0.0 0.0 11.0935 par=n axs= 0. 0. 1 rad=d1 ext=d2 erg=d3
si1= 0.0 2.77374
sp1= -21 1
si2= 0.0 .171047
sp2= 0 1
si3 H 0.0e0 2.5e-1 5.0e-1 7.5e-1 1.0e0
      1.25e0 1.5e0 1.75e0 2.0e0 2.25e0
      2.5e0 2.75e0 3.0e0 3.25e0 3.5e0
      3.75e0 4.0e0 4.25e0 4.5e0 4.75e0
      5.0e0 5.25e0 5.5e0 5.75e0 6.0e0 6.25e0
      6.5e0 6.75e0 7.0e0 7.25e0 7.5e0 7.75e0
      8.0e0 8.25e0 8.5e0 8.75e0 9.0e0
      9.25e0 9.5e0 9.750e0  1.00e1
 sp3 D 0 1.556e-1 1.980e-1 2.215e-1 2.123e-1 1.179e-1
      3.586e-2 1.255e-2 7.672e-3 5.505e-3 4.789e-3
      4.202e-3 3.659e-3 3.166e-3 2.724e-3
      2.331e-3 1.986e-3 1.686e-3 1.425e-3
      1.201e-3 1.009e-3 8.450e-4 7.060e-4
       5.884e-4 4.893e-4 4.060e-4 3.363e-4
      2.780e-4 2.294e-4 1.890e-4 1.555e-4
       1.277e-4 1.048e-4 8.584e-5
      7.024e-5 5.740e-5 4.686e-5
      3.821e-5 3.113e-5 2.533e-5 2.060e-5
c si3= L 2 3 4 5 6 7
c sp3= 9.689e-11 6.6025e-5 1.15499e-6 .971065 2.39294e-2
4.93867e-3
c IPOL 2 -1 1 1 0 0 18 214 215 216 217 218 219 220 221 222 223
224 225
c       226 227 228 229 230 231
c ******************************
c Material Definition
c ******************************
m1000      92233     -1.92e-8           $ U/TRU Ingot
         92234     -3.65e-4
         92235     -9.02e-3
         92236     -6.425e-3
         92237     -6e-12
         92238     -.984
         94238     -6.80e-13
         94239     -1.25e-11
         94240     -3.55e-12
         94241     -4.41e-13
         94242     -2.36e-12
         94243     -8.91e-28
         94244     -2.54e-16
m2000    48106     .0125
         48108     .0089
         48110     .1249
         48111     .1280
         48112     .2413
         48113     .1222
         48114     .2873
```

```
         48116     .0749
m3000 7014.70c     0.8      8016.70c    0.2  $ air
m4000 1001.70c     2.0      6000.70c   1.0   $ polyethylene
mt4000     poly.10t
c STAINLESS-STEEL
c       Cr number density = 1.6540e-2
c       Fe number density = 6.3310e-2
c       Ni number density = 6.5100e-3
c    total number density = 8.6360e-2
c
c
m5000 24050  7.1866e-4     $ Cr-50  4.345%
      24052  1.3859e-2     $ Cr-52 83.789%
      24053  1.5715e-3     $ Cr-53  9.501%
      24054  3.9117e-4     $ Cr-54  2.365%
      26054  3.7005e-3     $ Fe-54  5.845%
      26056  5.8090e-2     $ Fe-56 91.754%
      26057  1.3415e-3     $ Fe-57  2.119%
      26058  1.7853e-4     $ Fe-58  0.282%
      28058  4.4318e-3     $ Ni-58 68.0769%
      28060  1.7071e-3     $ Ni-60 26.2231%
      28061  7.4207e-5     $ Ni-61  1.1399%
      28062  2.3661e-4     $ Ni-62  3.6345%
      28064  6.0256e-5     $ Ni-64  0.9256%
m6000 2003  1.0             $Helium 3
m7000 3006 .0182
      3007 .224
      19039 .161
      19040 2.07e-5
      19041 .0116
      17035 .410
      17037 .131
      11023 .0218
      92233 1.01e-10
      92234 2.87e-6
      92235 8.56e-5
      92236 6.08e-5
      92237 1.89e-13
      92238 .00924
      94238 1.16e-5
      94239 .000175
      94240 .0000487
      94241 .0000204
      94242 .000326
      94243 1.22e-20
      94244 3.48e-9
      96241 1.3e-11
      96242 1.45e-9
      96243 9.80e-8
      96244 1.23e-8
      96245 1.66e-9
      96246 2.15e-11
```

```
      96248 1.57e-12
f8:n (214 215 216 217 218 219 220 221 222 223 224 225 226 227 228
      229 230 231)
c  fm4 1 6000 1
c  sd4 1
ft8:n cap 2003 gate 400 6400
```

APPENDIX D- SAMPLE SCRIPT FOR MCNP6 FOR SPONTANEOUS FISSION SOURCE FOR CP FAILURE MODES

```
Model JCC-31 for High Level Neutron Coincidence Counting
c ******************************
c Cell Cards
c ******************************
100  1000 -19.1  -1 2 -3 imp:n=1 $Uranium Ingot
101  7000 -1.24  -1 3 -99 imp:n=1 $Salt Entrained
110  2000 -8.65   -2 4 -7 imp:n=1 $Cadmium SHield
120  3000 -.0013   -1 -5 99 imp:n=1 $ Surrounding Air In Sample
Compartment
130  3000 -.0013   1 -7 2 -5  imp:n=1$ Surrounding Air In Sample
Compartment
140  2000 -8.65    -7 5 -6 imp:n=1 $ Cadmium Shield
150  4000 -0.92    6 -8 -7 imp:n=1 $Poly Reflector
160  5000 8.636e-2 -13 8 -9 imp:n=1 $Stainless Steel Electronics
170  2000 -8.65    7 -11 12 -8 imp:n=1 $Cadmium Shield
180  4000 -0.92    -7 -4 12 imp:n=1 $Poly Reflector
190  4000 -0.92    11 -10 12 -8 14 15 16 17 18 19 20 21
                   22 23 24 25 26 27 28 29 30 31 imp:n=1 $Poly
Reflector
314  4000 -0.92    32 -8 -14 imp:n=1    $Poly Reflector
315  4000 -0.92    32 -8 -15 imp:n=1    $Poly Reflector
316  4000 -0.92    32 -8 -16 imp:n=1    $Poly Reflector
317  4000 -0.92    32 -8 -17 imp:n=1    $Poly Reflector
318  4000 -0.92    32 -8 -18 imp:n=1    $Poly Reflector
319  4000 -0.92    32 -8 -19 imp:n=1    $Poly Reflector
320  4000 -0.92    32 -8 -20 imp:n=1    $Poly Reflector
321  4000 -0.92    32 -8 -21 imp:n=1    $Poly Reflector
322  4000 -0.92    32 -8 -22 imp:n=1    $Poly Reflector
323  4000 -0.92    32 -8 -23 imp:n=1    $Poly Reflector
324  4000 -0.92    32 -8 -24 imp:n=1    $Poly Reflector
325  4000 -0.92    32 -8 -25 imp:n=1    $Poly Reflector
326  4000 -0.92    32 -8 -26 imp:n=1    $Poly Reflector
327  4000 -0.92    32 -8 -27 imp:n=1    $Poly Reflector
328  4000 -0.92    32 -8 -28 imp:n=1    $Poly Reflector
329  4000 -0.92    32 -8 -29 imp:n=1    $Poly Reflector
330  4000 -0.92    32 -8 -30 imp:n=1    $Poly Reflector
331  4000 -0.92    32 -8 -31 imp:n=1    $Poly Reflector
200  2000 -8.65   -13 10 12  -8 imp:n=1 $Cadmium SHield
214  6000 -.0001785 -14 12 -32 imp:n=1  $He-3 Detector
215  6000 -.0001785 -15 12 -32 imp:n=1 $He-3 Detector
216  6000 -.0001785 -16 12 -32 imp:n=1  $He-3 Detector
217  6000 -.0001785 -17 12 -32 imp:n=1  $He-3 Detector
218  6000 -.0001785 -18 12 -32 imp:n=1  $He-3 Detector
219  6000 -.0001785 -19 12 -32 imp:n=1  $He-3 Detector
220  6000 -.0001785 -20 12 -32 imp:n=1  $He-3 Detector
221  6000 -.0001785 -21 12 -32 imp:n=1  $He-3 Detector
222  6000 -.0001785 -22 12 -32 imp:n=1  $He-3 Detector
```

```
223  6000 -.0001785 -23 12 -32 imp:n=1  $He-3 Detector
224  6000 -.0001785 -24 12 -32 imp:n=1  $He-3 Detector
225  6000 -.0001785 -25 12 -32 imp:n=1  $He-3 Detector
226  6000 -.0001785 -26 12 -32 imp:n=1  $He-3 Detector
227  6000 -.0001785 -27 12 -32 imp:n=1  $He-3 Detector
228  6000 -.0001785 -28 12 -32 imp:n=1  $He-3 Detector
229  6000 -.0001785 -29 12 -32 imp:n=1 $He-3 Detector
230  6000 -.0001785 -30 12 -32 imp:n=1  $He-3 Detector
231  6000 -.0001785 -31 12 -32 imp:n=1  $He-3 Detector
210  0             13:-12:9 imp:n=0 $Outside World

c ******************************
c Surface Cards Defining Detector
c ******************************
1 cz 2.7734
2 pz 0
3 pz 11.0935
4 pz -0.04
5 pz 40.6
6 pz 40.64
7 cz 8.5
8 pz 54.85
9 pz 65.85
10 cz 17
11 cz 8.54
12 pz  -14.25
13 cz 17.04
14 c/z 11 0 1.27
15 c/z -11 0 1.27
16 c/z 10.3366 3.7622 1.27
17 c/z 8.4625 7.0707 1.27
18 c/z 5.5 9.5263 1.27
19 c/z 1.910 10.8329 1.27
20 c/z -1.910 10.8329 1.27
21 c/z -5.5 9.5263 1.27
22 c/z -8.4265 7.0707 1.27
23 c/z -10.3366 3.7622 1.27
24 c/z -10.3366 -3.7622 1.27
25 c/z -8.4625 -7.0707 1.27
26 c/z -5.5 -9.5623 1.27
27 c/z  -1.9101 -10.8329 1.27
28 c/z 1.9101 -10.8329 1.27
29 c/z 5.5 -9.5263 1.27
30 c/z 8.4265  -7.0707 1.27
31 c/z 10.3366 -3.7622 1.27
32 pz 36.55
99 pz 11.26455

c ******************************
c Data Cards
c ******************************
c Source Definition
```

```
mode n
nps 1e6
sdef pos= 0.0 0.0 11.0935 par=sf axs= 0. 0. 1 rad=d1 ext=d2
$erg=d3
si1= 0.0 2.7734
sp1= -21 1
si2= 0.0 .171047
sp2= 0 1
c si3 H 0.0e0 2.5e-1 5.0e-1 7.5e-1 1.0e0
c      1.25e0 1.5e0 1.75e0 2.0e0 2.25e0
c      2.5e0 2.75e0 3.0e0 3.25e0 3.5e0
c      3.75e0 4.0e0 4.25e0 4.5e0 4.75e0
c      5.0e0 5.25e0 5.5e0 5.75e0 6.0e0 6.25e0
c      6.5e0 6.75e0 7.0e0 7.25e0 7.5e0 7.75e0
c      8.0e0 8.25e0 8.5e0 8.75e0 9.0e0
c      9.25e0 9.5e0 9.750e0  1.00e1
c sp3 D 0 1.554e-1 1.977e-1 2.198e-1 2.098e-1 1.173e-1
c      3.643e-2 1.311e-2 8.239e-3 6.018e-3 5.242e-3
c      4.6e-3 4.006e-3 3.466e-3 2.982e-3
c      2.552e-3 2.175e-3 1.845e-3 1.56e-3
c      1.315e-3 1.104e-3 9.252e-4 7.73e-4
c       6.443e-4 5.358e-4 4.446e-4 3.682e-4
c      3.044e-4 2.512e-4 2.070e-4 1.703e-4
c       1.399e-4 1.147e-4 9.4e-5
c      7.691e-5 6.286e-5 5.132e-5
c      4.185e-5 3.409e-5 2.774e-5 2.256e-5
c si3= L 2 3 4 5 6 7
c sp3= 9.689e-11 6.6025e-5 1.15499e-6 .971065 2.39294e-2
4.93867e-3
c IPOL 2 -1 1 1 0 0 18 214 215 216 217 218 219 220 221 222 223
224 225
c       226 227 228 229 230 231
c ******************************
c Material Definition
c ******************************
m1000      92233     -1.92e-8           $ U/TRU Ingot
         92234     -3.65e-4
         92235     -9.02e-3
         92236     -6.425e-3
         92237     -6e-12
         92238     -.984
         94238     -6.80e-13
         94239     -1.25e-11
         94240     -3.55e-12
         94241     -4.41e-13
         94242     -2.36e-12
         94243     -8.91e-28
         94244     -2.54e-16
m2000    48106     .0125
         48108     .0089
         48110     .1249
         48111     .1280
```

```
         48112     .2413
         48113     .1222
         48114     .2873
         48116     .0749
m3000 7014.70c     0.8      8016.70c    0.2  $ air
m4000 1001.70c     2.0      6000.70c   1.0   $ polyethylene
mt4000     poly.10t
c STAINLESS-STEEL
c       Cr number density = 1.6540e-2
c       Fe number density = 6.3310e-2
c       Ni number density = 6.5100e-3
c    total number density = 8.6360e-2
c
c
m5000 24050  7.1866e-4     $ Cr-50  4.345%
      24052  1.3859e-2     $ Cr-52 83.789%
      24053  1.5715e-3     $ Cr-53  9.501%
      24054  3.9117e-4     $ Cr-54  2.365%
      26054  3.7005e-3     $ Fe-54  5.845%
      26056  5.8090e-2     $ Fe-56 91.754%
      26057  1.3415e-3     $ Fe-57  2.119%
      26058  1.7853e-4     $ Fe-58  0.282%
      28058  4.4318e-3     $ Ni-58 68.0769%
      28060  1.7071e-3     $ Ni-60 26.2231%
      28061  7.4207e-5     $ Ni-61  1.1399%
      28062  2.3661e-4     $ Ni-62  3.6345%
      28064  6.0256e-5     $ Ni-64  0.9256%
m6000 2003  1.0             $Helium 3
m7000 3006 .0182
      3007 .224
      19039 .161
      19040 2.07e-5
      19041 .0116
      17035 .410
      17037 .131
      11023 .0218
      92233 1.01e-10
      92234 2.87e-6
      92235 8.56e-5
      92236 6.08e-5
      92237 1.89e-13
      92238 .00924
      94238 1.16e-5
      94239 .000175
      94240 .0000487
      94241 .0000204
      94242 .000326
      94243 1.22e-20
      94244 3.48e-9
      96241 1.3e-11
      96242 1.45e-9
      96243 9.80e-8
```

```
      96244 1.23e-8
      96245 1.66e-9
c      96246 2.15e-11
c      96248 1.57e-12
f8:n (214 215 216 217 218 219 220 221 222 223 224 225 226 227 228
      229 230 231)
c  fm4 1 6000 1
c  sd4 1
ft8:n cap 2003 gate 400 6400
```

LIST OF REFERENCES

[1] B. B. Cipiti, F. A. Duran, B. Key, Y. Liu, I. Lozano and R. Ward, "Modeling and Design of Integrated Safeguards and Security for an Electrochemical Reprocessing Facility," Sandia National Labs, Albuquerque, 2012.

[2] T. Burr and etal., "Roles for Process Monitoring in Nuclear Safeguards at Aqueous Reprocessing Plants," *Journal of Nuclear Materials Management,* pp. 42-52, 2012.

[3] H. Garcia, M. Simpson, W. Lin, T. Yoo and R. Carlson, "Detecting Proliferation Activities via System-Centric Integration and Interpretation of Multi-Modal Data Collected from a System of Sensors," in *Proceedings of the 54th Annual INMM Meeting*, Palm Desert, 2013.

[4] International Atomic Energy Agency, "IAEA Safeguards Glossary," IAEA, Vienna, 2001.

[5] J. M. Whitaker, *Safeguarding Uranium Enrichment: The Challenge of Large Gas Centrifuge Facilities*, Oak Ridge, Tennessee: ORNL, 2011.

[6] M. Ehinger and S. Johnson, "Lessons Learned in International Safeguards—Implementation of Safeguards," Oak Ridge National Laboratory, Oak Ridge, 2009.

[7] T. Burr, M. Hamada and C. Orton, "Data-Driven Versus Period-Driven Change Detection for Process Monitoring," in *Proceeding of the 53rd Annual Institute for Nuclear Materials Management Meeting*, Orlando, 2012.

[8] R. Avenhaus and J. Jaech, "On subdividing material balances in time and/or space," *Journal of Nuclear Materials Management,* vol. 10, no. 3, pp. 24-32, 1981.

[9] H. Garcia, W.-C. Lin and T.-S. Yoo, "Process Monitoring for Safeguards Via Even Generation, Integration, and Interpretation," in *Proceeds of the 51st Annual Institute for Nuclear Materials Management Meeting*, Baltimore, 2010.

[10] Nuclear Energy Agency, "Pyrochemical Separations in Nuclear Applications," Organization for Economic Cooperation and Development, Paris, 2004.

[11] R. Benedict, C. Solbrig, B. Westphal, T. Johnson, S. Li, K. Marsden and K. Goff, "Pyroprocessing Progress at Idaho National Laboratory," Idaho National Laboratory, Idaho Falls, 2007.

[12] H. Lee, G. Park, J.-W. Lee, K.-H. Kang, J.-M. Hur, J.-G. Kim, S. K.-T. Paek and I.-J. Cho, "Current Status of Pyroprocessing Development at KAERI," *Science and Technology of Nuclear Installations,* vol. 43, no. 4, pp. 317-328, 2011.

[13] T. Koyama, Y. Sakamura, M. Izuka, T. Kato, T. Murakami and J.-P. Glatz, "Development of Pyro-processing Fuel Cycle Technology for CLosing Actinide Cycle," *Procedia Chemistry,* vol. 7, no. 1, pp. 772-778, 2012.

[14] L. Cassayre, R. Malmbeck, M. Harrison, G. DeAngelis, C. Caravaca and S. Bourg, "Pyrochemical Separation of Spent Nuclear Fuel: Advances in the Frame of the European ASCEPT Project," in *Proceedings of the 2012 International Pyroprocessing Research Conference,* Fontana, 2012.

[15] M. Williamson and J. Willit, "Pyroprocessing Flowsheets for Recycling Used Nuclear Fuel," *Nuclear Engineering and Technology,* vol. 43, no. 4, pp. 329-333, 2011.

[16] U.S. Army, "Failure Modes, Effects and Criticality Analysis (FMECA) for Command, Control, Communications, Computer, Intelligence, Surveillance, and Reconnaisance (C4ISR) Facilities," US Army, Washington D.C., 2006.

[17] D. Stamatis, Failure Mode and Effect Analysis: FMEA from Theoy to Execution, Milwaukee: ASQ Quality Press, 2003.

[18] M. Krick and H. Menlove, "High-level neutron coincidence counter (HLNCC): users' manual," Los Alamos National Labs, Los Alamos, 1979.

[19] T. Lee, H. Kim, K. Jung and S. Park, "Status and Prospect of Safeguards by Design for the Pyroprocessing Facility," International Atomic Energy Agency, Vienna, 2010.

[20] R. Hoover, P. Lafreniere and E. Blandford, "Commercial-Scale Electrorefiner Failure Modes and Implications for Operations and Safeguards," in *American Nuclear Society Transactions*, Reno, 2014.

[21] S. Li and M. Simpsons, "Anocid Process of Electrorefining Spent Driver Fuel in Molten LiCl-KCl-UCl3/Cd System," *Journal of Minerals & Metallurgical Processing,* vol. 22, no. 4, pp. 192-198, 2005.

[22] R. Cumberland, R. Hoover, S. Phongikaroon and M.-S. Y, "Analysis of Equilibirium Methods for the Computation Model of the Mark-IV Electrorefiner," *Nuclear*

Engineering and Technology, vol. 43, no. 6, pp. 547-556, 2011.

[23] M. Iizuka, K. Uozumi, T. Ogata, T. Omori and T. Tsukada, "Development of an Innovative Electrorefiner for High Uranium Recovery Rate from Metal Fast Reactor Fuels," *Journal of Science and Technology,* vol. 46, no. 7, pp. 699-716, 2009.

[24] J. Lee, Y. Kang, S. Hwang, H. Lee, E. Kim and S. Park, "Assesment of a Hihg-Throughput Electrorefining Concept for a Spent Metallic Nuclear Fuel-I: Computational Fluid Dynamics Analysis," *Nuclear Technology,* vol. 162, no. 1, pp. 107-116, 2008.

[25] S. Li, "Experimental Observations on the Roles of the Cadmium Pool in the Mark-IV Electrorefiner," *Nuclear Technology,* vol. 162, no. 1, p. 144, 2008.

[26] B. Westphal, K. Mardsen, J. Price and L. D.V., "On the Development of a Distillation Process for the Electrometallurgical Treatment of Irradiated Spent Nuclear Fuel," *Nuclear Engineering and Technology,* vol. 40, no. 3, pp. 163-174, 2008.

[27] J. Jang, H. Kang, Y. Lee, L. H. and a. K. J.G., "Development of a Continous Ingot Casting Process for Uranium Dendrites in Pyroprocess," *Journal of Radionanalytical and Nuclear Chemistry,* vol. 295, no. 1, pp. 1743-1751, 2013.

[28] R. Cumberland and M.-S. Yim, "Development of a 1D Transient Electrorefiner Model for Pyrprocess Simulations," in *Transactions of the American Nuclear Society,* Washington D.C., 2011.

[29] R. Cumberland, "1D and 3D Simulation of Electrochemical Behavior of U/UCl3 and Pu/PuCl3 in Molten Salt Systems (Thesis)," Korean Advanced Institute of Science and Technology, Daejon, 2013.

[30] B.-.. Park, "A Time-Dependent Simulation of Molten Salt Electrolysis for Nuclear Wastes Transmutation (Dissertation)," Seoul National University, Seoul, 1999.

[31] D. B. Pelowtiz, "MCNPX User's Manual," Los Alamos, Los Alamos, 2011.

[32] S. Bowman and I. Gauld, "OrigenArp Primer: How to Perform Isotopic Depletion and Decay Calculations with SCALE/ORIGEN," Oak Ridge National Labs, Oak Ridge, 2010.

[33] Knoll Atomic Power Laboratory, Nuclides and Isotopes Sixteenth Edition, Schenectady: KAPL, 2002.

[34] E. Padovani, S. Pozzi, S. Clarke and E. Miller, "MCNPX-PoliMi User's Manual," Los Alamos, Los Alamos, 2010.

[35] W. Wilson, R. Perry, E. Shores, W. Charlton, T. Parish, G. Estest, T. Brown, E. Arthur, Bozoianm N, T. England, D. Madland and J. Stewart, "SOURCES 4C: A code for Calculating (alpha,n), Spontaneous Fission, and Delayed Neutron Sources and Spectra," Los Alamos, Los Alamos, 2002.

[36] J. Taylor, An Introduction to Error Analysis, Sausilito: University Science Books, 1997.

[37] B. R.A., "Use of Curium Spontaneous Fission Neutrons for Safeguardability of Remotely-Handled Nuclear Facilities: Fuel Fabrication in Pyroprocessing," *Nuclear Engineering and Design,* vol. 260, no. 1, pp. 64-77, 2013.

[38] J. Ackerman, "Chemical Basis for Pyrochemical Reprocessing of Nuclear Fuel," *Industrial & Engineering Chemistry Research,* vol. 30, no. 1, pp. 141-145, 1991.

[39] P. Lafreniere, D. Rappleye, R. Hoover, M. Simpson and E. Blandford, "Modeling Non-Destructive Assay Based Signatures for Application to Safeguarding Pyroprocessing," in *Proceedings of ICAPP*, Charlotte, 2014.

[40] P. Lafreniere, D. Rappleye, R. Hoover, M. Simpson and E. Blandford, "Application of Signature- Based Safeguards to Electrorefining and the Ingot Casting Process," *Nuclear Technology,* Accepted with Revisions May 2014.

[41] P. Lafreniere, R. Hoover and E. Blandford, "Determination of Pyroprocessing Cathode Processor Failure Modes and Intregation into a Signature-Based Safeguards (SBS) Framework," in *Proceeding of INMM Meeting*, Atlanta, 2014.